The effect of forest structure on yellow pine/mixed-conifer resilience to wildfire and bark beetle disturbance in the Sierra Nevada, California

By

MICHAEL J. KOONTZ

DISSERTATION

Submitted in partial satisfaction of the requirements for the degree of

DOCTOR OF PHILOSOPHY

in

ECOLOGY

in the

OFFICE OF GRADUATE STUDIES

of the

UNIVERSITY OF CALIFORNIA
DAVIS

Approved:

_____

(Andrew M. Latimer), Chair

_____

(Malcolm P. North)

_____

(Constance I. Millar)

Committee in Charge

2019

i

The effect of forest structure on yellow pine/mixed-conifer resilience to wildfire and

bark beetle disturbance in the Sierra Nevada, California

To my mom and dad.

Acknowledgements

I want to start by acknowledging that all of this work took place on unceded territory of a number of Native American peoples including the Patwin, Ute, Nisenan, Washoe, Mono, Miwok, and Paiute. Their ongoing history is intimately tied to forest disturbances in the Sierra Nevada yellow pine/mixed-conifer and greatly contributes to what is considered the 'natural range of variation' for this system. Changes in disturbance regimes since Euroamerican invasion must therefore be considered within the context of settler colonialism, which dramatically shifted the Native American influence on these disturbance-prone landscapes. I am grateful for the opportunity to live and do science in these areas.

I am very grateful for the many people that supported me during my Ph.D. There's a lot of overlap in the various ways that people have contributed to my experience in the Graduate Group in Ecology (GGE), which speaks to the diversity of talent represented by my colleagues.

The best thing I did during my PhD was to join a pair of exceptional labs. The collegiality and immense talent of the Latimer and North labs kept me excited to pursue awesome science. I'm grateful to the Latimer Lab members with whom I overlapped: Jens Stevens, Derek Young, Brian Smithers, Allie Weill, Marina LaForgia, and Paige Kouba. I'm also grateful to the North Lab members with whom I overlapped: Mason Earles, Brian Smithers, Gabina Bohlmann, Jens Stevens, Jan Ng, Max Odland, and Paige Kouba.

Thank you to the administrative staff that helped me keep track of all the logistics associated with completing a PhD: Holly Hatfield Rogai, Elizabeth Sturdy, Matt Malepeai, and Lisa Brown. I don't know how I would have kept up with the various deadlines, paperwork, funding sources, etc. without your help.

Thanks to Leif Mortenson for taking me on my first tour of western pine beetle attacked forests as well as Chris Fettig for guiding my thinking on how this disturbance affects Sierra Nevada forests. Thanks to Brandon Collins for early conversations about yellow pine/mixed-conifer fire regimes and measuring forest structural heterogeneity.

Thanks to the GLORIA Great Basin nonprofit for an amazing time in the mountains collecting important baseline data about alpine plant distributions. This is a long-term monitoring project and I hope to be volunteering with you all for the next 100 years.

Thanks to Dan Krofcheck, Alex Mandel, and Taylor Nelson for letting me bounce ideas off of you while I was building the drone project.

Thanks to all the people that are coauthors on manuscripts I led during my PhD: Chhaya Werner, Steve Fick, Zack Steel, Leif Mortenson, Chis Fettig, Ruth Hufbauer, Brett Melbourne, Meagan Oldfather, Malcolm North, and Andrew Latimer.

I learned a ton about teaching during my time at UC Davis in large part due to my participation with The Carpentries and the R-DAVIS class. I want to thank a series of folks that helped guide my learning about modern pedagogical approaches to teaching scientific computing skills including Noam Ross, Michael Levy, Myfanwy Johnston, Greg Wilson, Tracy Teal, Titus Brown, Emilio Laca, Ryan Peek, Taylor Reiter, Martha Wohlfeil, Michael Culshaw-Maurer, and Andrew Latimer. A special shoutout to Titus Brown for letting me co-run an R bootcamp during the Data Intensive Biology Summer Institute and Ryan Peek for inviting me to go all-in with him on building a scientific computing course in the GGE based on a shared motivation to lower the barrier to entry for using computers to help folks do ecology.

Michael J. Koontz
June 2019
ECOLOGY

Abstract

Past and future disturbances are linked by their feedbacks with forest structure– the size, species, and spatial distribution of vegetation in a forest. Disturbances like wildfire and bark beetle activity can alter forest structure, which then influences the outcomes of future disturbances. The long-term persistence of forest ecosystems hinges on these feedbacks, which promotes resilience– the ability of a system to absorb disturbances and still retain its essential identity and functions. I explore these feedbacks by measuring disturbance severity as well as local-scale forest structure at broad spatial extents in the yellow pine/mixed-conifer forest system of the Sierra Nevada, California. I bring new tools, such as massively parallel cloud-based GIS and drone remote sensing, to bear on questions about how forest structure affects wildfire and bark beetle disturbance in this region. I introduce a new framework to describe how wildfire suppression biases burning conditions and thus observed fire effects in large fire events to be more extreme than would be expected if all ignitions were allowed to burn. With this selection bias of large fires in mind, I generate a new dataset of fire effects in the Sierra yellow pine/mixed-conifer system that captures outcomes from smaller fire events. I use this new fire effects dataset and also measure variability in horizontal forest structure using the computer vision approach of texture analysis for nearly 1000 fires that burned in the system between 1984 and 2017. I find that greater variability in forest structure reduces the probability of high severity wildfire, which increases forest resilience in this system ill-adapted to recover from large high-severity events. Finally, I use drone-captured imagery and structure from motion (SfM) techniques to recreate complex forest structure of over 9 km^2 of western

pine beetle-attacked forest along a 350 km latitudinal gradient and a 1000 m elevation gradient. I found that availability of the host tree for the western pine beetle, ponderosa pine, increases the probability of ponderosa pine mortality and average host size plays a different role depending on the climatic water deficit (a proxy for tree moisture stress) at each site: at cool wet sites, more small hosts drive mortality; at hot dry sites, more large hosts drive mortality. Overall, this work demonstrates how an understanding the complexities of local forest structure, including the size, species, and spatial distribution of trees, can generate new insights into how broader-scale patterns of tree mortality arise during wildfire and bark beetle disturbance.

Contents

List of Tables

List of Figures

Chapter 1

Local variability of vegetation structure increases forest resilience to wildfire

Michael J. Koontz[1,2,*], Malcolm P. North[2,3], Chhaya M. Werner[2,4], Stephen E. Fick[5,6], Andrew M. Latimer[2]

[1]Graduate Group in Ecology, University of California; Davis, CA

[2]Department of Plant Sciences, University of California; Davis, CA

[3]Pacific Southwest Research Station, U.S.D.A. Forest Service; Davis, CA

[4]Center for Population Biology, University of California; Davis, CA

[5]U.S. Geological Survey, Southwest Biological Science Center

[6]Department of Ecology and Evolutionary Biology, University of Colorado; Boulder, CO

Abstract

The long-term persistence of forest ecosystems hinges on their resilience to ongoing disturbance. Quantification of resilience in these valuable ecosystems remains difficult due to their vast extent and the longevity of forest species. Resilience to wildfire may arise from feedback between fire behavior and vegetation structure, which dictates fuel loading and continuity. Regular fire generates structural variability which may then enable forests to withstand future fires and retain their fundamental properties and functions– a hallmark of a resilient system. A century of fire suppression in the western United States has homogenized the structure of many forests, potentially upsetting these feedbacks and compromising forest resilience. We investigate the generality and scale of the effect of structural variability on wildfire behavior in yellow pine/mixed-conifer forest of California's Sierra Nevada using cloud computing and texture analysis of a 33-year time series of satellite imagery. We measure wildfire response to forest structure for an unprecedented number and size range of wildfires, ensuring representation of both typical and extreme fire behavior, and find that greater structural variability is strongly associated with a lower probability of fire-induced overstory tree mortality. This resistance to wildfire was most apparent at the smallest spatial extent of forest structure tested (90m x 90m). Local-scale structural variability thus links past and future fire behavior, and makes forests more resilient to wildfire disturbance. Management strategies that increase vegetation structural variability, such as allowing fires to burn under moderate fuel and weather conditions, may therefore increase the probability of long-term forest persistence.

Significance

A "resilient" forest endures disturbance and is likely to persist. Resilience to wildfire may derive from variability in vegetation structure, which interrupts fuel continuity and prevents fire from killing overstory trees. Testing the generality and scale of this phenomenon is challenging because forests are vast, long-lived ecosystems. We develop a novel cloud computing approach to consistently quantify forest structural variability and fire severity across >30 years and nearly 1,000 wildfires in California's Sierra Nevada. We find that greater small-scale structural variability increases resilience by reducing rates of fire-induced tree mortality. Resilience of these forests is likely compromised by structural homogenization from a century of fire suppression, but may be restored with management that increases structural variability of vegetation.

Introduction

Biological systems comprising heterogeneous elements can retain their fundamental properties in the face of regular disturbance. This ability of a heterogeneous system to absorb disturbances, reorganize, and to persist within a domain of stability with respect to its identity, structure, function, and feedbacks is termed resilience (Holling 1973, Walker et al. 2004). Resilience has been demonstrated in complex biological systems characterized by a variety of different types of "heterogeneity" including genetic diversity (Reusch et al. 2005, Baskett et al. 2009, Agashe 2009), species diversity (Tilman 1994, Chesson 2000, Cadotte et al. 2013), functional diversity (Gazol and Camarero 2016), topoclimatic complexity (Ackerly et al. 2010, Lenoir et al. 2013), and temporal environmental variation (Questad and Foster 2008). An emerging paradigm in forest ecology is that resilience to

disturbances such as wildfire and insect outbreaks may arise from spatial variability in the structure of vegetation (Stephens et al. 2008, North et al. 2009, Virah-Sawmy et al. 2009).

In much of the western United States, forests are experiencing "unhealthy" conditions which compromise their resilience and leaves them prone to catastrophic shifts in ecosystem type (Millar and Stephenson 2015). Warmer temperatures coupled with recurrent drought (i.e., "hotter droughts") exacerbate water stress on trees (Williams et al. 2013, Millar and Stephenson 2015, Clark et al. 2016) and a century of fire suppression has drastically increased forest density and structural homogeneity (Safford and Stevens 2017, Stevens et al. 2017). Combined, these changes are liable to upset the feedbacks between forest structure and pattern-forming ecological disturbances that historically stabilized the system and made it resilient. In the yellow pine/mixed-conifer forests of California's Sierra Nevada mountain range, wildfires kill much larger contiguous patches of trees than in the several centuries prior to Euroamerican settlement making natural forest regeneration after these megafires uncertain (Miller and Thode 2007, Safford and Stevens 2017, Stevens et al. 2017, Steel et al. 2018). Forests are essential components of the biosphere with high management priority given their large carbon stores and other valued ecosystem services (Hansen et al. 2013, Millar and Stephenson 2015, Trumbore et al. 2015, Crowther et al. 2015), making it critical to understand how and at what scale spatial structural variability affects forest resilience to disturbance.

Resilience of forest ecosystems is fundamentally challenging to quantify because forests comprise long-lived species, span large geographic extents, and are affected by disturbances at a broad range of spatial scales. The ease or difficulty with which a disturbance changes a system's state is termed resistance, and it is a key component of resilience (Walker et al. 2004) (though some treatments in forest ecology define "resistance" as a

distinct process from "resilience"; see Millar et al. (2007)). To assess a forest's resistance, the relevant state change to measure is the loss of its characteristic native biota– overstory trees (Keith et al. 2013). Using this framework, a forest system that is resistant to wildfire should generally experience less overstory tree mortality when a fire occurs.

Wildfire behavior is inherently complex and is influenced by local weather, topography, and fuel conditions created by a legacy of disturbances at any particular place (Sugihara et al. 2006). For instance, high surface fuel loads and presence of "ladder fuels" in the understory increase the probability of "crowning" fire behavior, which kills a high proportion of trees (Agee and Skinner 2005, Stephens et al. 2008). A structurally variable forest can largely avoid overstory tree mortality because discontinuous fuel loads interrupt crown fire spread, reduced amounts of accumulated ladder fuel decreases the probability of crowning, and because small tree clumps with fewer trees don't facilitate self-propagating fire behavior (Graham et al. 2004, Scholl and Taylor 2010). In fire-prone forests with relatively intact fire regimes and high structural variability such as in the Jeffrey pine/mixed-conifer forests of the Sierra San Pedro Mártir in Baja, California, there tends to be reduced vegetation mortality after wildfires compared to fire-suppressed forests (Stephens et al. 2008). Thus, more structurally variable forests are predicted to persist due to their resistance to inevitable wildfire disturbance (Graham et al. 2004, Moritz et al. 2005, Stephens et al. 2008). However, it has been difficult to test this foundational concept at broad spatial extents, or resolve at what scale variability in forest structure is meaningful for resilience (Kotliar and Wiens 1990).

Wildfire severity typically describes the proportion of vegetation mortality resulting from fire, and can be measured by comparing pre- and postfire satellite imagery for a specific area. This usually requires considerable manual effort for image collation and processing, followed by calibration with field data (Miller and Thode 2007, Miller et al. 2009, De

Santis et al. 2010, Cansler and McKenzie 2012, Veraverbeke and Hook 2013, Parks et al. 2014, Prichard and Kennedy 2014, Edwards et al. 2018, Fernández-García et al. 2018). Efforts to measure severity across broad spatial extents, such as the Monitoring Trends in Burn Severity project (Eidenshink et al. 2007), are motivated by and fulfill management needs in response to individual fires but are unsuitably subjective for characterizing patterns and trends across large numbers of wildfires (Kolden et al. 2015). Automated efforts to remotely assess wildfire have arisen, but they tend to focus on more aggregate measures of wildfire such as whether an area burned or the probability that it burned rather than the severity of the burn (Bastarrika et al. 2011, Goodwin and Collett 2014, Boschetti et al. 2015, Hawbaker et al. 2017), but see (Reilly et al. 2017, Parks et al. 2018). Here, we present a method to automate the measurement of wildfire severity using minimal user inputs: a geometry of interest (a wildfire perimeter or a field plot location) and an alarm date (the date the fire was discovered). This information is readily available in many fire-prone areas (such as California, via the Fire and Resource Assessment Program; http://frap.fire.ca.gov/projects/fire_data/fire_perimeters_index) or could be derived using existing products (such as the Landsat Burned Area Essential Climate Variable product described in Hawbaker et al. (2017)).

Vegetation characteristics can be measured using remotely-sensed imagery (Rouse et al. 1973, Asner et al. 2016, Young et al. 2017). Texture analysis of these vegetation characteristics can quantify ecologically relevant local environmental heterogeneity across broad spatial extents (Wood et al. 2012, Stein et al. 2014, Huang et al. 2014, Tuanmu and Jetz 2015), which may be used as a direct measure of ecosystem resilience (Kéfi et al. 2014). Developed for image classification and computer vision, texture analysis characterizes each pixel in an image by a summary statistic of its neighboring pixels, and represents a measure of local heterogeneity which itself varies across the landscape (Haralick et al.

1973). Texture analysis of forested areas detects heterogeneity of overstory vegetation, which corresponds to fuel loading and continuity, capturing the primary influence of vegetation structure on fire behavior.

We use freely-available Landsat satellite data and a new image processing approach to calculate wildfire severity for nearly 1,000 wildfires encompassing a wide size range (down to 4 hectares) and long time series (1984 to 2017) of Sierra Nevada wildfires that burned in yellow pine/mixed-conifer forest. The larger fires that comprise most severity databases are often able to grow large only after escaping initial suppression efforts and burning under extreme fuel and weather conditions (Calkin et al. 2005). We better represent non-extreme fire behavior by measuring severity across a wider range of fire sizes, allowing us to characterize general features of wildfire behavior in this system without bias. We calibrate 56 configurations of our algorithmic approach to ground-based wildfire severity measurements, and select the best performing severity metric to generate a comprehensive, system-wide severity dataset. We pair the resulting extensive database of wildfire severity measures with image texture analysis of vegetation to ask: (1) Does spatial variability in forest structure increase the resilience of California yellow pine/mixed-conifer forests by reducing the severity of wildfires? (2) At what scale does structural variability have the strongest association with wildfire severity? and (3) Does the influence of structural variability on fire severity depend on topography, regional climate, or other conditions?

Results

We found that the remotely sensed relative burn ratio (RBR) metric of wildfire severity measured across a 48-day interval prior to the wildfire discovery date correlated best
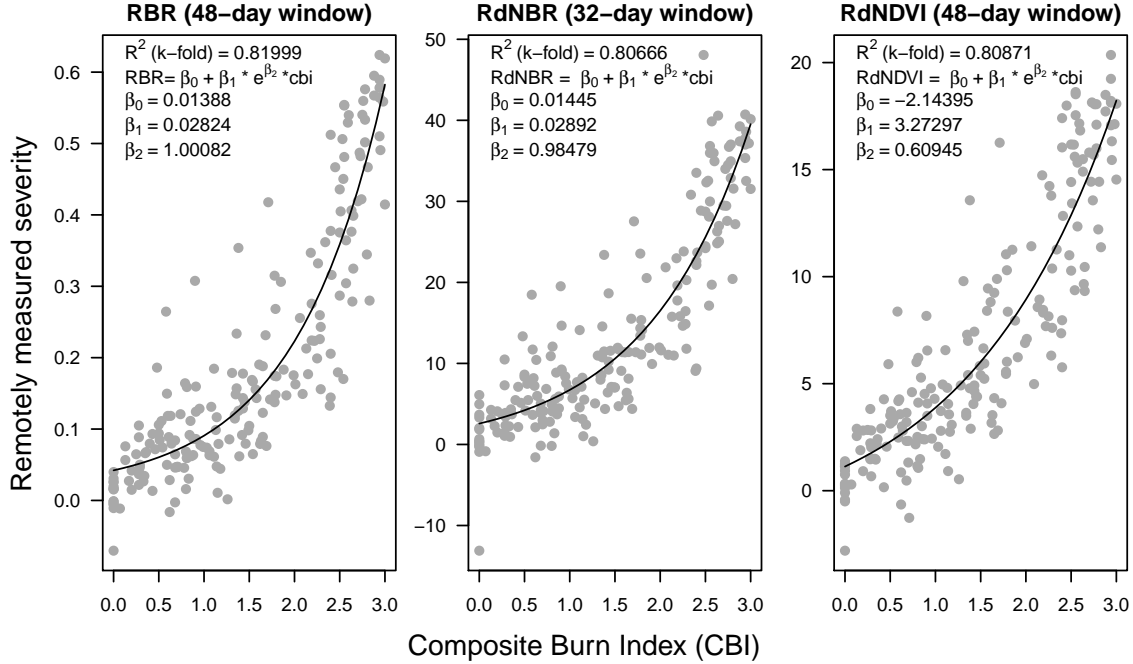
Figure 1.1: Three top performing remotely-sensed severity metrics based on 5-fold cross validation (relative burn ratio, 48-day window, bicubic interpolation; relative delta normalized burn ratio, 32-day window, bilinear interpolation; and relative delta normalized difference vegetation index, 48-day window, bilinear interpolation) calculated using new automated image collation algorithms, calibrated to 208 field measures of fire severity (composite burn index). See Supplemental Table 1 for performance of all tested models.

with ground-based composite burn index (CBI) measurements of severity (5-fold cross validation $R^2 = 0.82$; Figure 1; Supp. Table 1). Our method to calculate remotely sensed severity using automated Landsat image fetching performs as well or better than most other reported methods that use hand-curation of Landsat imagery (see review in Edwards et al. (2018)). Further, several combinations of remotely sensed severity metrics, time windows, and interpolation methods validate well with the ground-based severity metrics, including those based on NDVI which is calculated using reflectance in shorter wavelengths than those typically used for measuring severity (Figure 1). The top three configurations of our remotely sensed severity metric are depicted in Figure 1. Based on these model comparisons, we used the relative burn ratio (RBR) calculated

using a 48-day time window before the fire and bicubic interpolation as our metric of severity. We created the boolean response variable representing whether the sampled point burned at high-severity or not by determining whether the RBR exceeded 0.282, the threshold for high-severity derived using the non-linear relationship in Equation 1 (Figure 1).

Neighborhood size effect

Table 1.1: Comparison of four models described in Eq. 2 using different neighborhood sizes for calculating forest structural variability (standard deviation of NDVI within the neighborhood), neighborhood mean NDVI, and topographic roughness. LOO is a measure of a model's predictive accuracy (with lower values corresponding to more accurate prediction) and is calculated as -2 times the expected log pointwise predictive density (elpd) for a new dataset (Vehtari et al. 2017). ΔLOO is the difference between a model's LOO and the lowest LOO in a set of models (i.e., the model with the best predictive accuracy). The Bayesian R^2 is a 'data-based estimate of the proportion of variance explained for new data' (Gelman et al. 2018). Note that Bayesian R^2 values are conditional on the model so shouldn't be compared across models, though they can be informative about a single model at a time.

Model	Neighborhood size for variability measure	LOO (-2*elpd)	Δ LOO to best model	SE of Δ LOO	LOO model weight (%)	Bayesian R^2
1	90m x 90m	40786	0	NA	100	0.299
2	150m x 150m	40842	56.03	14.69	0	0.298
3	210m x 210m	40883	96.87	20.94	0	0.297

Model	Neighborhood size for variability measure	LOO (-2*elpd)	Δ LOO to best model	SE of Δ LOO	LOO model weight (%)	Bayesian R^2
4	270m x 270m	40912	125.9	24.73	0	0.297

The model with the best out-of-sample prediction accuracy assessed by leave-one-out cross validation was the model fit using the smallest neighborhood size for the variability of forest structure (standard deviation of neighborhood NDVI), the mean of neighborhood NDVI, and the terrain roughness (standard deviation of elevation) (Table 1). Model weighting based on the LOO score suggests 100% of the model weight belongs to the model using the smallest neighborhood size window.

Effects of prefire vegetation density, 100-hour fuel moisture, potential annual heat load, and topographic roughness on wildfire severity

We report the results from fitting the model described in Equation 2 using the smallest neighborhood size (90m x 90m) because this was the best performing model (see above) and because the size and magnitude of estimated coefficients were similar across neighborhood sizes (Supp. Table 2).

We found that the strongest influence on the probability of a forested area burning at high-severity was the density of the vegetation, as measured by the prefire NDVI at that central pixel. A greater prefire NDVI led to a greater probability of high-severity fire ($\beta_{\text{prefire\_ndvi}} = 1.044$; 95% CI: [0.911, 1.174]); Figure 2). There was a strong negative
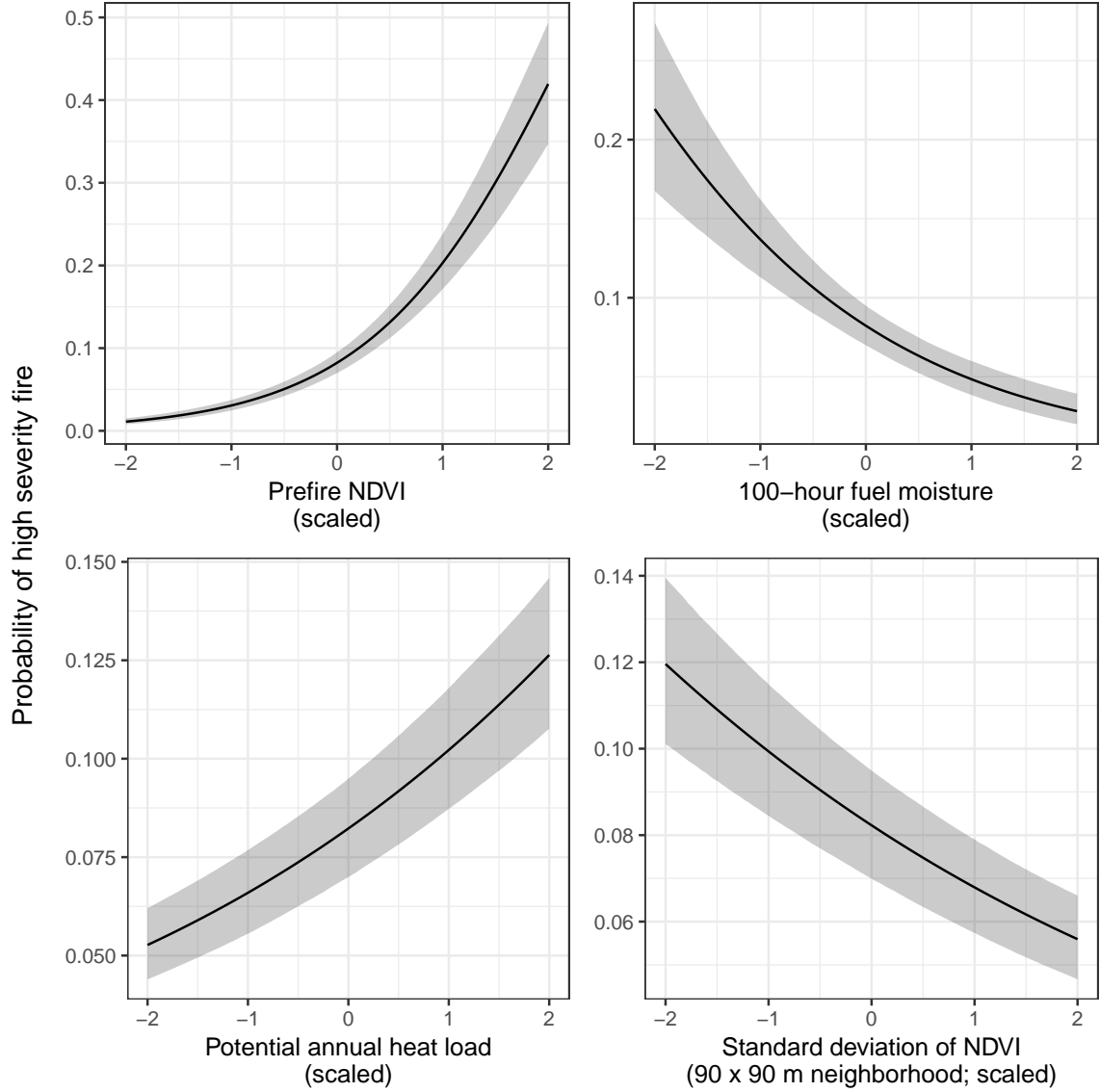
Figure 1.2: The main effects and 95% credible intervals of the covariates having the strongest relationships with the probability of high-severity fire. All depicted relationships derive from the model using the 90m x 90m neighborhood size window for neighborhood standard deviation of NDVI, neighborhood mean of NDVI, and topographic roughness, as this was the best performing model of the four neighborhood sizes tested. The effect sizes of these covariates were similar for each neighborhood size tested.

relationship between 100-hour fuel moisture and wildfire severity such that increasing 100-hour fuel moisture was associated with a reduction in the probability of a high-severity wildfire (β_{fm100} = -0.569; 95% CI: [-0.71, -0.423]) (Figure 2). Potential annual heat load, which integrates aspect, slope, and latitude, also had a strong positive relationship with the probability of a high-severity fire. Areas that were located on southwest facing sloped terrain at lower latitudes had the highest potential annual heat load, and they were more likely to burn at high-severity (β_{pahl} = 0.239; 95% CI: [0.208, 0.271]) Figure 2). We found no effect of local topographic roughness on wildfire severity ($\beta_{\text{topographic\_roughness}}$ = -0.01; 95% CI: [-0.042, 0.022]). We found a negative effect of the prefire neighborhood mean NDVI on the probability of a pixel burning at high-severity ($\beta_{\text{nbhd\_mean\_NDVI}}$ = -0.14; 95% CI: [-0.278, 0.002]). This is in contrast to the positive effect of the prefire NDVI of the pixel itself.

There was also a strong negative interaction between the neighborhood mean NDVI and the prefire NDVI of the central pixel ($\beta_{\text{nbhd\_mean\_NDVI*prefire\_NDVI}}$ -0.573; 95% CI: [-0.62, -0.526]).

Effect of variability of vegetation structure on wildfire severity

We found strong evidence for a negative effect of variability of vegetation structure on the probability of a high-severity wildfire ($\beta_{\text{nbhd\_stdev\_NDVI}}$ = -0.208; 95% CI: [-0.247, -0.17]); Figure 2). We also found significant interactions between variability of vegetation structure and prefire NDVI $\beta_{\text{nbhd\_stdev\_NDVI*prefire\_NDVI}}$ = 0.125; 95% CI: [0.029, 0.218]) as well as between variability of vegetation structure and neighborhood mean NDVI ($\beta_{\text{nbhd\_stdev\_NDVI*nbhd\_mean\_NDVI}}$ = -0.129; 95% CI: [-0.223, -0.034]).

Discussion

Broad-extent, fine-grain, spatially-explicit analyses of whole ecosystems are key to illuminating macroecological phenomena (Heffernan et al. 2014). We used a powerful, cloud-based geographic information system and data repository, Google Earth Engine, as a 'macroscope' (Beck et al. 2012) to study feedbacks between vegetation structure and wildfire disturbance in yellow pine/mixed-conifer forests of California's Sierra Nevada mountain range. With this approach, we reveal and quantify general features of this forest system, and gain deeper insights into the mechanisms underlying its function.

Factors influencing the probability of high-severity wildfire

We found that the strongest influence on the probability of high-severity wildfire was prefire NDVI. Greater NDVI corresponds to high canopy cover and vegetation density (Rouse et al. 1973) which translate directly to live fuel loads in the forest canopy and can increase high severity fire (Parks et al. 2018). Critically, overstory canopy cover and density also correlate with surface fuel loads (Lydersen et al. 2015, Collins et al. 2016), which play a larger role in driving high severity fire compared to canopy fuel loads in these forests (Stephens et al. 2012). Thus NDVI is likely a strong predictor of fire severity because it is correlated with both surface fuel loads and canopy live fuel density.

We found a strong positive effect of potential annual heat load as well as a strong negative effect of 100-hour fuel moisture, results which corroborates similar studies (Parks et al. 2018). Some work has shown that terrain ruggedness (Holden et al. 2009), and particularly coarser-scale terrain ruggedness (Dillon et al. 2011), is an important predictor of wildfire severity, but we found no effect using our measure of terrain ruggedness.

DISCUSSION

Critically, we found a strong negative effect of forest structural variability on wildfire severity that was opposite in direction but similar in magnitude to the effect of potential annual heat load. Just as the positive effect of NDVI is likely driven by surface fuel loads, the negative effect of variability in NDVI (our measure of structural variability), is likely driven by discontinuity in surface fuel loads, which can reduce the probability of initiation and spread of tree-killing crown fires (Wagner 1977, Agee and ForestResourcesU 1996, Graham et al. 2004, Agee and Skinner 2005).

Feedback between forest structural variability and wildfire severity

This system-wide inverse relationship between structural variability and wildfire severity closes a feedback that links past and future fire behavior via forest structure. Frequent, mixed-severity wildfire generates variable forest structure (North et al. 2009, Larson and Churchill 2012, Malone et al. 2018), which in turn, as we demonstrate, dampens the severity of future fire. In contrast, exclusion of wildfire homogenizes forest structure and increases the probability that a fire, when it occurs, will produce large, contiguous patches of overstory mortality (Stevens et al. 2017, Steel et al. 2018). The proportion and spatial configuration of fire severity in fire-prone forests are key determinants of their long-term persistence (Stevens et al. 2017, Steel et al. 2018). Lower-severity fire or scattered patches of higher-severity fire reduce the risk of conversion to a non-forest vegetation type (Stevens et al. 2017, Walker et al. 2018), while prospects for forest regeneration are bleak when high-severity patch sizes are much larger than the natural range of variation for the system (Wagtendonk 2006, Stephens et al. 2009, Millar and Stephenson 2015, Coppoletta et al. 2016, Safford and Stevens 2017, Miller and Safford 2017, Stevens et al. 2017). Thus, the forest-structure-mediated feedback between past and future fire

15

severity underlies the resilience of the Sierra Nevada yellow pine/mixed-conifer system.

Neighborhood size

We found that the effect of a forest patch's neighborhood characteristics on the probability of high-severity fire was strongest at the smallest neighborhood size that we tested, 90m x 90m. This suggests that the moderating effect of variability in vegetation structure on fire severity is a very local phenomenon. This corroborates work by Safford et al. (2012), who found that crown fires (with high tree killing potential) were almost always reduced to surface fires (with low tree killing potential) within 70m of entering an fuel reduction treatment area.

At a landscape level, forest treatments that reduce fuel loads and increase structural variability can be effective at reducing fire severity across broader spatial scales (Stephens et al. 2009). This may reflect that severity patterns for a whole fire are an emergent property of very local interactions between forest structure and fire behavior. Some work suggests that the scale of these interactions may depend on even broader-scale effects of fire weather, with small-scale variability failing to influence fire behavior under extreme conditions (Peters et al. 2004, Lydersen et al. 2014), though we did not detect such an interaction. The notion of emergent patterns of severity arising from local effects of vegetation structure is supported by work on fuel reduction treatments, which suggests that fire behavior can be readily modified with forest structural changes to only 20% (when strategically located) to 60% (when randomly located) of the landscape (Graham et al. 2004).

DISCUSSION

Correlation between covariates and interactions

Unexpectedly, we found a strong interaction between the prefire NDVI at a pixel and its neighborhood mean NDVI. These two variables are strongly correlated (Spearman's $\rho =$ 0.97), so the general effect of this interaction is to dampen the dominating effect of prefire NDVI. Thus, though the marginal effect of prefire NDVI on the probability of high-severity fire is still positive and large, its real-world effect might be more comparable to other modeled covariates when including the negative main effect of neighborhood mean NDVI, the negative interaction effect of prefire NDVI and neighborhood mean NDVI, and their tendency to covary (compare the real-world effect of vegetation density: $\beta_{\text{prefire\_ndvi}} + \beta_{\text{nbhd\_mean\_NDVI}} + \beta_{\text{nbhd\_mean\_NDVI*prefire\_NDVI}} = 0.331$, to the effect of 100-hour fuel moisture, which becomes the effect with the greatest magnitude: $\beta_{\text{fm100}} =$ -0.569).

In the few cases when prefire NDVI and the neighborhood mean NDVI contrast, there is an overall effect of increasing the probability of high-severity fire. When prefire NDVI at the central pixel is high and the neighborhood NDVI is low (e.g., an isolated vegetation patch; Supplemental Fig. 2), the probability of high-severity fire is expected to dramatically increase. When prefire NDVI at the central pixel is low and the neighborhood NDVI is high (e.g., a hole in the center of an otherwise dense forest; Supplemental Fig. 2), the probability of high-severity fire at that central pixel is still expected to be fairly high even though there is limited vegetation density (see Supplemental Fig. 2). In these forest NDVI datasets, when these variables do decouple, they tend to do so in the "hole in the forest" case and lead to a greater probability of high-severity fire at the central pixel despite the lower vegetation density there. This can perhaps be explained if the consistently high vegetation density in a local neighborhood– itself more likely to burn

at high-severity– exerts a contagious effect on the central pixel, raising its probability of burning at high-severity regardless of how much fuel might be there to burn.

A new approach to remotely sensing wildfire severity

We developed a new approach to calculating wildfire severity leveraging the cloud-based data catalog, the large parallel processing system, and the distribution of computation tasks in Google Earth Engine to enable rapid high-throughput analyses of earth observation data (Gorelick et al. 2017). Our programmatic assessment of wildfire severity across the 972 Sierra Nevada yellow pine/mixed-conifer fires in the FRAP perimeter database, which required fetching thousands of Landsat images and performing dozens of calculations across them, was automated and took less than an hour to complete. We found that the relative burn ratio (RBR) calculated using prefire Landsat images collected over a 48-day period prior to the fire and postfire Landsat images collected over a 48-day period one year after the prefire images validated the best with ground-based severity measurements (composite burn index; CBI). Further, we found that this method was robust to a wide range of severity metrics, time windows, and interpolation techniques.

Most efforts to calculate severity from satellite data rely on hand curation of a single prefire and a single postfire image (Miller and Thode 2007, Miller et al. 2009, De Santis et al. 2010, Cansler and McKenzie 2012, Veraverbeke and Hook 2013, Parks et al. 2014, Prichard and Kennedy 2014, Edwards et al. 2018, Fernández-García et al. 2018). Recently, Parks et al. (2018) found that using a composite of several prefire images and several postfire images to detect fire impacts performed at least as well as using a single pre- and postfire image. Using composite images also facilitated automated image fetching. Parks et al. (2018) used 3- to 4-month windows during pre-specified times of the year (depending on the fire's region) to collate pre- and postfire imagery one year before

the fire and one year after. In contrast, we tested multiple time window lengths based on the fire start date regardless of when it burned during the year. Basing our pre- and postfire image fetching on fixed lengths of time since the fire start date standardized the amount of time elapsed in each severity assessment. Our best remotely sensed severity configuration used a much shorter time window compared to Parks et al. (2018) (48 days versus 3 to 4 months), which likely balanced an incorporation of enough imagery to be representative of the pre- and postfire vegetation conditions but not so many images that different phenological conditions across the time window added noise to each composite.

Many algorithms have been developed to measure fire effects on vegetation in an attempt to better correspond to field data (Key and Benson 2006, Miller and Thode 2007, Parks et al. 2014). We found that several other remotely sensed measures of severity, including one based on NDVI that is rarely deployed, validated nearly as well with ground-based data as the best configuration (RBR calculated using a 48-day time window). We echo the conclusion of Zhu et al. (2006) that the validation of differences between pre- and postfire NDVI to field measured severity data, which uses near infrared reflectance, is comparable to validation using more commonly used severity metrics (e.g., RdNBR and RBR) that rely on short wave infrared reflectance. One immediately operational implication of this is that the increasing availability of low-cost small unhumanned aerial systems (sUAS a.k.a. drones) and near-infrared-detecting imagers (e.g., those used for agriculture monitoring) may be used to reliably measure wildfire severity at very high spatial resolutions.

Conclusions

While the severity of a wildfire in any given place is controlled by many variables, we have presented strong evidence that, across large areas of forest, variable forest structure generally makes yellow pine/mixed-conifer forest in the Sierra Nevada more resistant

to this inevitable disturbance. It has been well-documented that frequent, low-severity wildfire maintains forest structural variability. Here, we demonstrate a system-wide reciprocal effect suggesting that greater local-scale variability of vegetation structure makes fire-prone, dry forests more resilient to wildfire and may increase the probability of their long-term persistence.

Material and Methods

Study system

Our study assesses the effect of vegetation structure on wildfire severity in the Sierra Nevada mountain range of California in yellow pine/mixed-conifer forests (Figure 3). This system is dominated by a mixture of conifer species including ponderosa pine (*Pinus ponderosa*), sugar pine (*Pinus lambertiana*), incense-cedar (*Calocedrus decurrens*), Douglas-fir (*Pseudotsuga menziesii*), white fir (*Abies concolor*), and red fir (*Abies magnifica*), angiosperm trees primarily including black oak (*Quercus kelloggii*), as well as shrubs (Safford and Stevens 2017). We considered "yellow pine/mixed-conifer forest" to be all areas designated as a yellow pine, dry mixed-conifer, or moist mixed-conifer pre-settlement fire regime (PFR) in the USFS Fire Return Interval Departure database (https://www.fs.usda.gov/detail/r5/landmanagement/gis/?cid=STELPRDB5327836), which reflects potential vegetation and is less sensitive to recent land cover change (Steel et al. 2018). We considered the Sierra Nevada region to be the area within the Sierra Nevada Foothills, the High Sierra Nevada, and the Tehachapi Mountain Area Jepson ecoregions (JepsonFloraProject 2016).
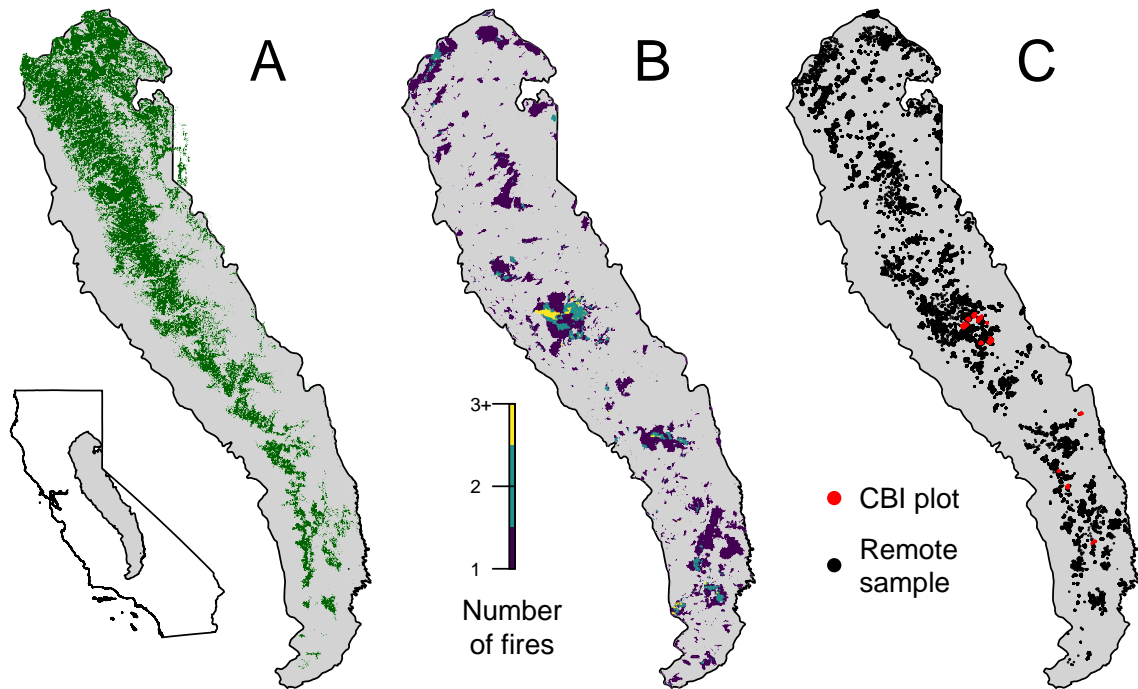
Figure 1.3: Geographic setting of the study. A) Location of yellow pine/mixed-conifer forests as designated by the Fire Return Interval Departure (FRID) product which, among other things, describes the potential vegetation in an area based on the pre-Euroamerican settlement fire regime. B) Locations of all fires covering greater than 4 hectares that burned in yellow pine/mixed-conifer forest between 1984 and 2017 in the Sierra Nevada mountain range of California according to the State of California Fire Resource and Assessment Program database, the most comprehensive database of fire perimeters of its kind. Colors indicate how many fire perimeters overlapped a given pixel within the study time period. C) (red) Locations of 208 composite burn index (CBI) ground plots used to calibrate the remotely sensed measures of severity. (black) Locations of random samples drawn from 972 unique fires depicted in panel B that were in yellow pine/mixed-conifer forest as depicted in panel A, and which were designated as "burned" by exceeding a threshold relative burn ratio (RBR) determined by calibrating the algorithm presented in this study with ground-based CBI measurements.

A new approach to remotely sensing wildfire severity

We measured forest vegetation characteristics and wildfire severity using imagery from the Landsat series of satellites (Miller and Thode 2007, Eidenshink et al. 2007) with radiometric correction post-processing (Masek et al. 2006, Vermote et al. 2016, USGS 2017a, 2017b). Landsat satellites image the entire Earth approximately every 16 days with a 30m pixel resolution. We used Google Earth Engine, a massively parallel cloud-based geographic information system and image hosting platform, for all image collation and processing (Gorelick et al. 2017).

We calculated wildfire severity for the most comprehensive digital record of fire perimeters in California: The California Department of Forestry and Fire Protection, Fire and Resource Assessment Program (FRAP) fire perimeter database (http://frap.fire.ca.gov/projects/fire_data/fire_perimeters_index). The FRAP database includes all known fires that covered more than 4 hectares, compared to the current standard severity database in this region which only includes fires covering greater than 80 hectares (Miller and Thode 2007, Miller et al. 2012, Miller and Safford 2012, Steel et al. 2018). Using the FRAP database of fire perimeters, we quantified fire severity within each perimeter of 972 wildfires in the Sierra Nevada yellow pine/mixed-conifer forest that burned between 1984 and 2017. Our approach more than doubles the number of fire events represented from 430 to 972, though only increases the total burned area represented from 7.44e+05 to 7.69e+05 hectares because most of the additional fires are small. We use a consistent algorithmic approach to calculate fire severity across all fires, avoiding subjective judgements that some previous approaches have used to characterize severity separately for each fire.

MATERIAL AND METHODS

Fetching and processing pre- and postfire imagery

For each fire perimeter, we fetched a time series of prefire Landsat images starting the day before the fire alarm date and extending backward in time by a user-defined time window. An analogous postfire time series of Landsat imagery was fetched exactly one year after the date range used to filter the prefire collection. We tested 4 time windows: 16, 32, 48, or 64 days which were chosen to ensure that at least 1, 2, 3, or 4 Landsat images were captured by the date ranges (Supplemental Fig. 1). The Landsat archive we filtered included imagery from Landsat 4, 5, 7, and 8, so each pre- and postfire image collection may contain a mix of scenes from different satellite sources to enhance coverage. For each image in the pre- and postfire image collections, we masked pixels that were not clear (i.e., clouds, cloud shadows, snow, and water) using the CFMask algorithm (Foga et al. 2017).

For each Landsat image in the prefire and postfire collections, we calculated standard indices that capture vegetation cover and fire effects such as charring. Normalized difference vegetation index (NDVI) correlates with vegetation density, canopy cover, and leaf area index (Rouse et al. 1973). Normalized burn ratio (NBR) and normalized burn ratio version 2 (NBR2) respond strongly to fire effects on vegetation (García and Caselles 1991, Key and Benson 2006, USGS 2017b, 2017a, Hawbaker et al. 2017) (Equations in Supplemental Methods).

We composited each prefire image collection (including the pixel values representing NDVI, NBR, and NBR2) into a single prefire image and each postfire image collection into a single postfire image, by calculating the median of the unmasked values on a per-pixel basis across the stack of images in each pre- and postfire collection. Composite pre- and postfire images can be successfully used to measure wildfire severity instead of using

23

raw, individual images (Parks et al. 2018).

We composited each pre- and postfire image collection (including the pixel values representing NDVI, NBR, and NBR2) into a single pre- and postfire image using a median reducer, which calculated the median of the unmasked values on a per-pixel basis across the stack of images in each collection. Composite pre- and postfire images can be successfully used to measure wildfire severity instead of using raw, individual images (Parks et al. 2018).

Calculating wildfire severity

Using the compositing approach, we calculated the most commonly used metrics of remotely-sensed wildfire severity to validate against ground-based data: the relative burn ratio (RBR) (Parks et al. 2014), the delta normalized burn ratio (dNBR) (Miller and Thode 2007, Eidenshink et al. 2007), the relative delta normalized burn ratio (RdNBR) (Miller and Thode 2007, Miller and Safford 2012), the delta normalized burn ratio 2 (dNBR2) (Hawbaker et al. 2017), the relative delta normalized burn ratio 2 (RdNBR2), and the delta normalized difference vegetation index (dNDVI) (Eidenshink et al. 2007). We also calculate a new, analogous metric to the RdNBR using NDVI– the relative delta normalized difference vegetation index (RdNDVI). We calculated the delta severity indices (dNBR, dNBR2, dNDVI) without multiplying by a rescaling constant (e.g., we did not multiply the result by 1000 as in Miller and Thode (2007)). Following Reilly et al. (2017), we did not correct the delta indices using a phenological offset value, as our approach implicitly accounts for phenology by incorporating multiple cloud-free images across the same time window both before the fire and one year later. (Full equations can be found in the Supplemental Methods)

Example algorithm outputs are shown in Figure 4.
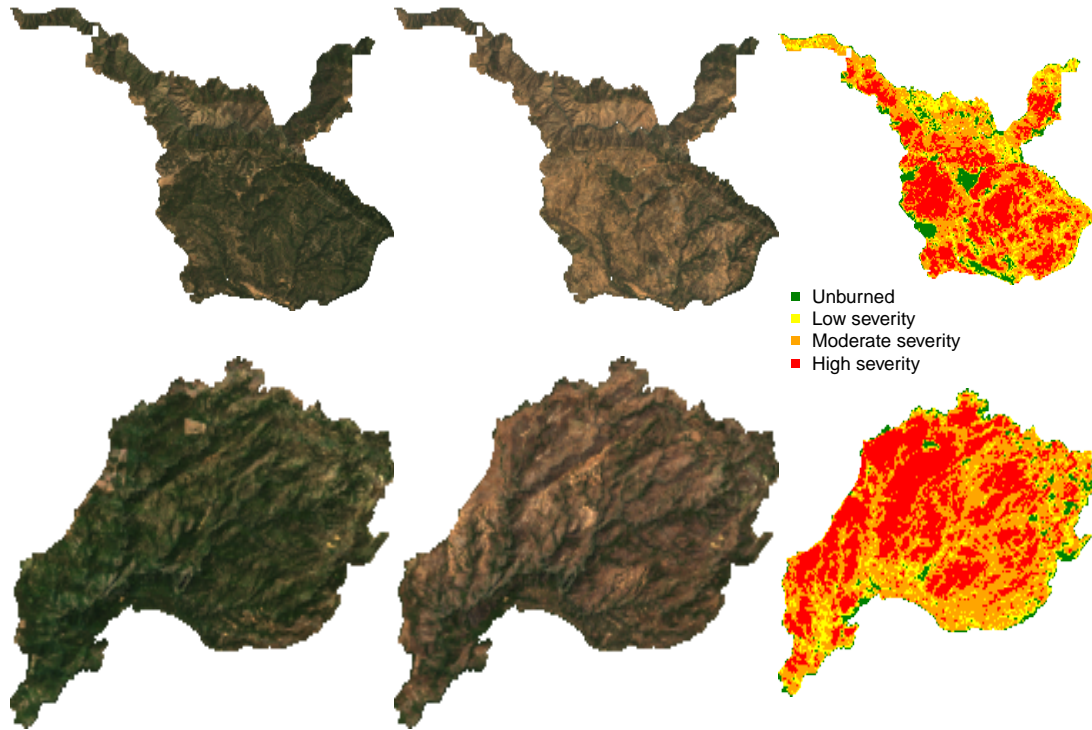
Figure 1.4: Example algorithm outputs for the Hamm Fire of 1987 (top half) and the American Fire of 2013 (bottom half) showing: prefire true color image (left third), postfire true color image (center third), relative burn ratio (RBR) calculation using a 48-day image collation window before the fire and one year later (right third). For visualization purposes, these algorithm outputs have been resampled to a resolution of 100m x 100m from their original resolution of 30m x 30m. Data used for analyses were sampled from the outputs at the original resolution.

Calibrating remotely-sensed wildfire severity with field-measured wildfire severity

We calibrated our remotely-sensed measure of wildfire severity with 208 field measures of overstory tree mortality from two previously published studies (Zhu et al. 2006, Sikkink et al. 2013) (Figure 3). The Composite Burn Index (CBI) is a metric of vegetation mortality across several vertical vegetation strata within a 30m diameter field plot (Key and Benson 2006). The CBI ranges from 0 (no fire impacts) to 3 (very high fire impacts), and has a long history of use as a standard for calibrating remotely-sensed severity data (Key and Benson 2006, Miller and Thode 2007, Miller et al. 2009, Cansler and McKenzie 2012, Parks et al. 2014, 2018, Prichard and Kennedy 2014). Following Miller and Thode (2007), Miller et al. (2009), Parks et al. (2014), and Parks et al. (2018), we fit a non-linear model to each remotely-sensed severity metric of the following form:

(1) $\text{remote\_severity} = \beta_0 + \beta_1 e^{\beta_2 \text{cbi\_overstory}}$

We fit the model in Equation 1 for all 7 of our remotely-sensed severity metrics (RBR, dNBR, RdNBR, dNBR2, RdNBR2, dNDVI, RdNDVI) using 4 different time windows from which to collate satellite imagery (16, 32, 48, and 64 days). Following Cansler and McKenzie (2012), Parks et al. (2014), and Parks et al. (2018), we used bilinear interpolation to extract remotely-sensed severity at the locations of the CBI field plots to better align remote and field measurements. We also extracted remotely-sensed severity values using bicubic interpolation. In total, we fit 56 models (7 severity measures, 4 time windows, 2 interpolation methods) and performed five-fold cross validation using the `modelr` and `purrr` packages in R (R Core Team 2018, Henry and Wickham 2019, Wickham 2019). To compare goodness of model fits with Miller and Thode (2007), Miller et al. (2009), and Parks et al. (2014), we report the average R^2 value from the five folds

for each of the 56 models.

Remote sensing other conditions

Vegetation structural variability

We used texture analysis to calculate a remotely-sensed measure of local forest variability (Haralick et al. 1973, Tuanmu and Jetz 2015). Within a moving square neighborhood window with sides of 90m, 150m, 210m, and 270m, we calculated forest variability for each pixel as the standard deviation of the NDVI values of its neighbors (not including itself). NDVI correlates well with foliar biomass, leaf area index, and vegetation cover (Rouse et al. 1973), so a higher standard deviation of NDVI within a given local neighborhood corresponds to discontinuous canopy cover and abrupt vegetation edges (see Figure 5) (Franklin et al. 1986). Canopy cover is positively correlated with surface fuel loads including dead and down wood, grasses, and short shrubs (Lydersen et al. 2015, Collins et al. 2016), which are primarily responsible for initiation and spread of "crowning" fire behavior which kills overstory trees (Stephens et al. 2012).

Topographic conditions

Elevation data were sourced from the Shuttle Radar Topography Mission (Farr et al. 2007), a 1-arc second digital elevation model. Slope and aspect were extracted from the digital elevation model. Per-pixel topographic roughness was calculated as the standard deviation of elevation values within the same-sized kernels as those used for variability in forest structure (90m, 150m, 210m, and 270m on a side and not including the central pixel).

We used the digital elevation model to calculate the potential annual heat load at each
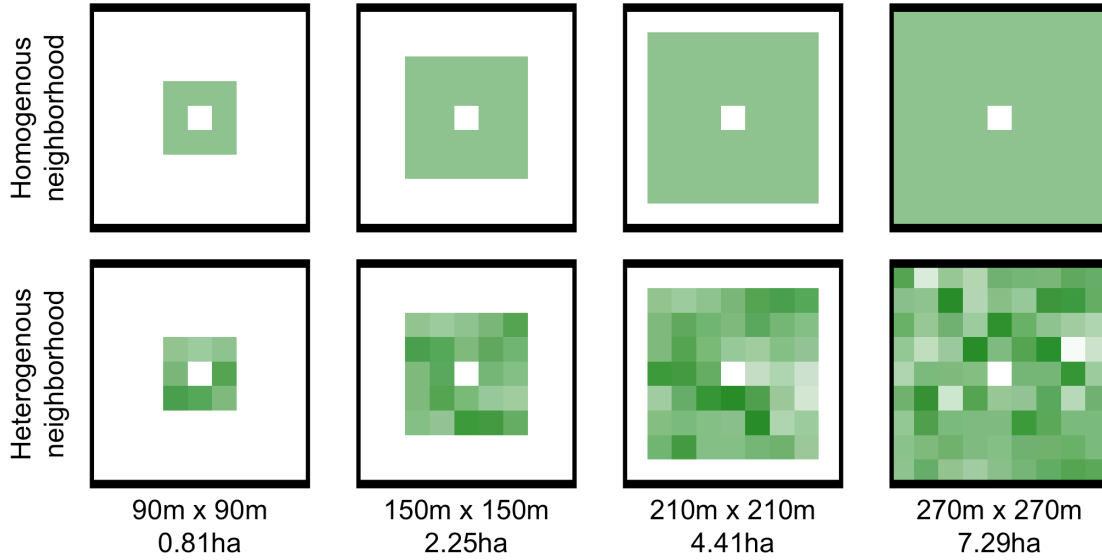
Figure 1.5: Example of homogenous forest (top row) and heterogenous forest (bottom row) with the same mean NDVI values (~0.6). Each column represents forest structural variability measured using a different neighborhood size.

pixel, which is an integrated measure of latitude, slope, and a folding transformation of aspect about the northeast-southwest line (McCune and Keon (2002) with correction in McCune (2007); See Supplemental Methods for equations)

Moisture conditions

The modeled 100-hour fuel moisture data were sourced from the gridMET product, a gridded meteorological product with a daily temporal resolution and a 4km x 4km spatial resolution (Abatzoglou 2013). We calculated 100-hour fuel moisture as the median 100-hour fuel moisture for the 3 days prior to the fire. The 100-hour fuel moisture is a correlate of the regional temperature and moisture which integrates the relative humidity, the length of day, and the amount of precipitation in the previous 24 hours. Thus, this measure is sensitive to multiple hot dry days across the 4km x 4km spatial extent of each grid cell, but not to diurnal variation in relative humidity nor to extreme weather events

during a fire.

Remote samples

Approximately 100 random points were selected within each FRAP fire perimeter in areas designated as yellow pine/mixed-conifer forest and the values of wildfire severity as well as the values of each covariate were extracted at those points using nearest neighbor interpolation. Using the calibration equation described in Equation 1 for the best configuration of the remote severity metric, we removed sampled points corresponding to "unburned" area prior to analysis (i.e., below an RBR threshold of 0.045). The random sampling amounted to 54109 total samples across 972 fires.

Modeling the effect of forest variability on severity

We used the Relative Burn Ratio (RBR) calculated using bicubic interpolation within a 48-day window to derive our response variable for analyses of forest structural variability, as it showed the best correspondence to field severity data measured as average R^2 in the 5-fold cross validation. Using the non-linear relationship between RBR and CBI from the best performing calibration model, we calculated the threshold RBR corresponding to "high-severity" signifying complete or near-complete overstory mortality (RBR value of 0.282 corresponding to a CBI value of 2.25). If the severity at a remote sample point was greater than this threshold, the point was scored as a 1. We used a hierarchical logistic regression model (Equation 2) to assess the probability of high-severity wildfire as a linear combination of the remote metrics described above: prefire NDVI of each pixel, standard deviation of NDVI within a neighborhood (i.e., forest structural variability), the mean NDVI within a neighborhood, 100-hour fuel moisture, potential annual heat

load, and topographic roughness. We included two-way interactions between the structural variability measure and prefire NDVI, neighborhood mean NDVI, and 100-hour fuel moisture. We include the two-way interaction between a pixel's prefire NDVI and its neighborhood mean NDVI to account for structural variability that may arise from differences between these variables (see Supplemental Fig. 2). We scaled all predictor variables, used weakly-regularizing priors, and estimated an intercept for each individual fire with pooled variance.

$$severity_{i,j} \sim Bern(\phi_{i,j})$$

$$(2) \quad logit(\phi_{i,j}) = \begin{aligned} &\beta_0 + \\ &\beta_{\text{nbhd\_stdev\_NDVI}} * \text{nbhd\_stdev\_NDVI}_i + \\ &\beta_{\text{prefire\_NDVI}} * \text{prefire\_NDVI}_i + \\ &\beta_{\text{nbhd\_mean\_NDVI}} * \text{nbhd\_mean\_NDVI}_i + \\ &\beta_{\text{fm100}} * \text{fm100}_i + \\ &\beta_{\text{pahl}} * \text{pahl}_i + \\ &\beta_{\text{topographic\_roughness}} * \text{topographic\_roughness}_i + \\ &\beta_{\text{nbhd\_stdev\_NDVI*fm100}} * \text{nbhd\_stdev\_NDVI}_i * \text{fm100}_i + \\ &\beta_{\text{nbhd\_stdev\_NDVI*prefire\_NDVI}} * \text{nbhd\_stdev\_NDVI}_i * \text{prefire\_NDVI}_i + \\ &\beta_{\text{nbhd\_stdev\_NDVI*nbhd\_mean\_NDVI}} * \text{nbhd\_stdev\_NDVI}_i * \text{nbhd\_mean\_NDVI}_i + \\ &\beta_{\text{nbhd\_mean\_NDVI*prefire\_NDVI}} * \text{nbhd\_mean\_NDVI}_i * \text{prefire\_NDVI}_i + \\ &\gamma_j \end{aligned}$$

$$\gamma_j \sim \mathcal{N}(0, \sigma_{\text{fire}})$$

MATERIAL AND METHODS

Assessing the relevant scale of forest variability

Each neighborhood size (90m, 150m, 210m, 270m on a side) was substituted in turn for the neighborhood standard deviation of NDVI, neighborhood mean NDVI, and terrain ruggedness covariates to generate a candidate set of 4 models. To assess the scale at which the forest structure variability effect manifests, we compared the 4 candidate models based on different neighborhood sizes using leave-one-out cross validation (LOO cross validation) (Vehtari et al. 2017). We inferred that the neighborhood size window used in the best-performing model reflected the scale at which the forest structure variability effect had the most support.

Statistical software

We used R for all statistical analyses (R Core Team 2018). We used the `brms` package to fit mixed effects models in a Bayesian framework which implements the No U-Turn Sampler (NUTS) extension to the Hamiltonian Monte Carlo algorithm (Hoffman and Gelman 2014, Bürkner 2017). We used 4 chains with 3000 samples per chain (1500 warmup samples and 1500 posterior samples) and chain convergence was assessed for each estimated parameter by ensuring Rhat values were less than or equal to 1.01 (Bürkner 2017).

Data availability

All data and analysis code are available via the Open Science Framework (DOI to be established) including a new dataset representing wildfire severity, vegetation characteristics, and regional climate conditions within the perimeters of 1,090 fires from the FRAP

database that burned in yellow pine/mixed-conifer forest in the Sierra Nevada, California between 1984 and 2017.

Acknowledgements

Chapter 2

Mathematics and Science

Math

TeX is the best way to typeset mathematics. Donald Knuth designed TeX when he got frustrated at how long it was taking the typesetters to finish his book, which contained a lot of mathematics. One nice feature of *R Markdown* is its ability to read LaTeX code directly.

If you are doing a thesis that will involve lots of math, you will want to read the following section which has been commented out. If you're not going to use math, skip over or delete this next commented section.

Chemistry 101: Symbols

Chemical formulas will look best if they are not italicized. Get around math mode's automatic italicizing in LaTeX by using the argument `$\mathrm{formula here}$`, with

your formula inside the curly brackets. (Notice the use of the backticks here which enclose text that acts as code.)

So, $Fe_2^{2+}Cr_2O_4$ is written `$\mathrm{Fe_2^{2+}Cr_2O_4}$`.

Exponent or Superscript: O^-

Subscript: CH_4

To stack numbers or letters as in Fe_2^{2+}, the subscript is defined first, and then the superscript is defined.

Bullet: $CuCl \bullet 7H_2O$

Delta: Δ

Reaction Arrows: $\longrightarrow$ or $\xrightarrow{solution}$

Resonance Arrows: $\leftrightarrow$

Reversible Reaction Arrows: $\rightleftharpoons$

Typesetting reactions

You may wish to put your reaction in an equation environment, which means that LaTeX will place the reaction where it fits and will number the equations for you.

$$C_6H_{12}O_6 + 6O_2 \longrightarrow 6CO_2 + 6H_2O \tag{2.1}$$

We can reference this combustion of glucose reaction via Equation (2.1).

Other examples of reactions

$NH_4Cl_{(s)} \rightleftharpoons NH_{3(g)} + HCl_{(g)}$

$$\text{MeCH}_2\text{Br} + \text{Mg} \xrightarrow[below]{above} \text{MeCH}_2 \bullet \text{Mg} \bullet \text{Br}$$
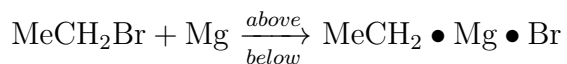
Physics

Many of the symbols you will need can be found on the math page http://web.reed.edu/cis/help/latex/math.html and the Comprehensive LaTeX Symbol Guide (http://mirror.utexas.edu/ctan/info/symbols/comprehensive/symbols-letter.pdf).

Biology

You will probably find the resources at http://www.lecb.ncifcrf.gov/~toms/latex.html helpful, particularly the links to bsts for various journals. You may also be interested in TeXShade for nucleotide typesetting (http://homepages.uni-tuebingen.de/beitz/txe.html). Be sure to read the proceeding chapter on graphics and tables.

Chapter 3

Tables, Graphics, References, and Labels

Tables

By far the easiest way to present tables in your thesis is to store the contents of the table in a CSV or Excel file, then read that file in to your R Markdown document as a data frame. Then you can style the table with the `kable` function, or functions in the kableExtra pacakge.

In addition to the tables that can be automatically generated from a data frame in **R** that you saw in [R Markdown Basics] using the `kable` function, you can also create tables using *pandoc*. (More information is available at http://pandoc.org/README.html#tables.) This might be useful if you don't have values specifically stored in **R**, but you'd like to display them in table form. Below is an example. Pay careful attention to the alignment in the table and hyphens to create the rows and columns. Generally I don't recommend this approach of typing the table directly into your R Markdown document.

Table 3.1: Correlation of Inheritance Factors for Parents
and Child

Factors	Correlation between Parents & Child	Inherited
Education	-0.49	Yes
Socio-Economic Status	0.28	Slight
Income	0.08	No
Family Size	0.18	Slight
Occupational Prestige	0.21	Slight

We can also create a link to the table by doing the following: Table 3.1. If you go back to [Loading and exploring data] and look at the `kable` table, we can create a reference to this max delays table too: Table **??**. The addition of the (`\#tab:inher`) option to the end of the table caption allows us to then make a reference to Table `\@ref(tab:label)`. Note that this reference could appear anywhere throughout the document after the table has appeared.

Figures

If your thesis has a lot of figures, *R Markdown* might behave better for you than that other word processor. One perk is that it will automatically number the figures accordingly in each chapter. You'll also be able to create a label for each figure, add a caption, and then reference the figure in a way similar to what we saw with tables earlier. If you label your figures, you can move the figures around and *R Markdown* will automatically adjust the numbering for you. No need for you to remember! So that you don't have to get too far into LaTeX to do this, a couple **R** functions have been created for you to assist. You'll see their use below.

In the **R** chunk below, we will load in a picture stored as `uw.png` in our main directory. We then give it the caption of "UW logo", the label of "uwlogo", and specify that this is a figure. Make note of the different **R** chunk options that are given in the R Markdown file (not shown in the knitted document). Here is a reference to the UW logo: Figure 3.1. Note the use of the `fig:` code here. By naming the **R** chunk that contains the figure, we can then reference that figure later as done in the first sentence here. We can also specify the caption for the figure via the R chunk option `fig.cap`.

Figure 3.1: UW logo
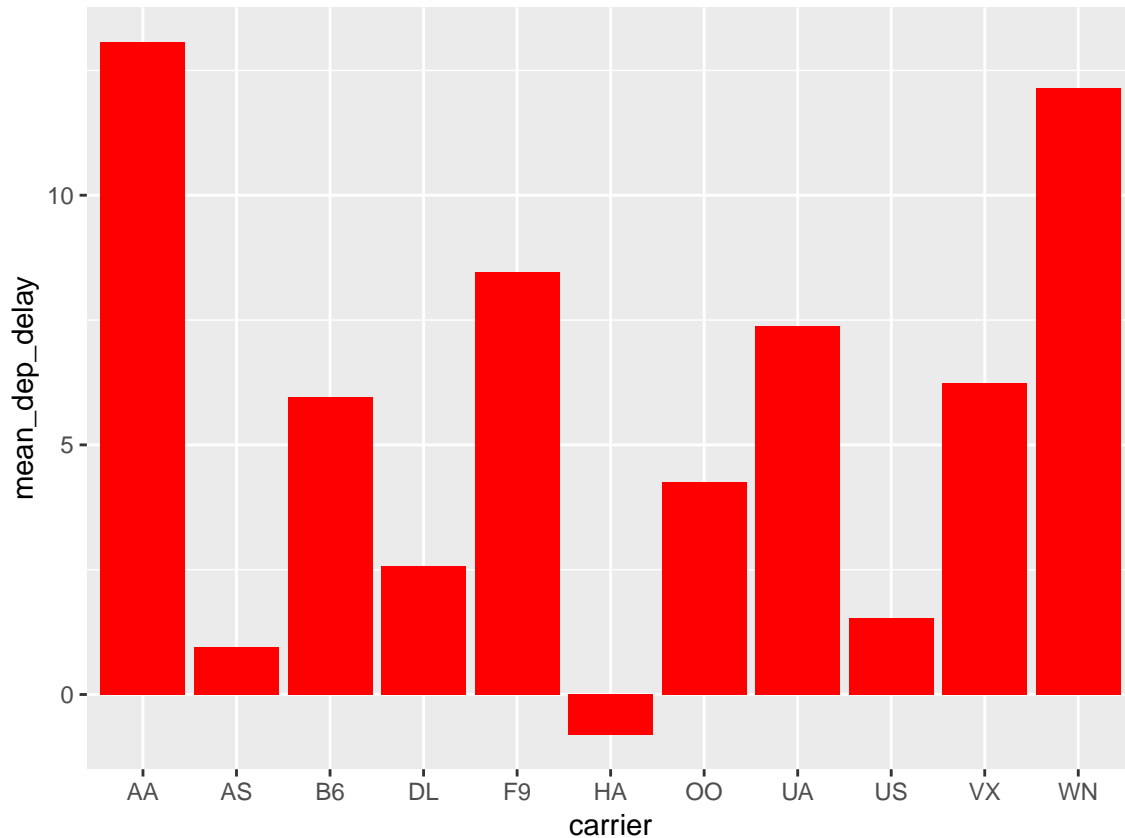
Figure 3.2: Mean Delays by Airline

Below we will investigate how to save the output of an **R** plot and label it in a way similar to that done above. Recall the `flights` dataset from Chapter **??**. (Note that we've shown a different way to reference a section or chapter here.) We will next explore a bar graph with the mean flight departure delays by airline from Portland for 2014. Note also the use of the `scale` parameter which is discussed on the next page. Here is a reference to this image: Figure 3.2.

A table linking these carrier codes to airline names is available at https://github.com/ismayc/pnwflights14/blob/master/data/airlines.csv.
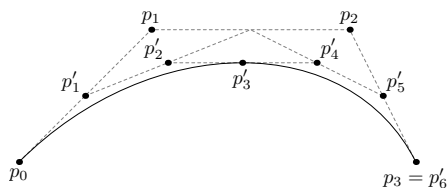
Figure 3.3: Subdiv. graph
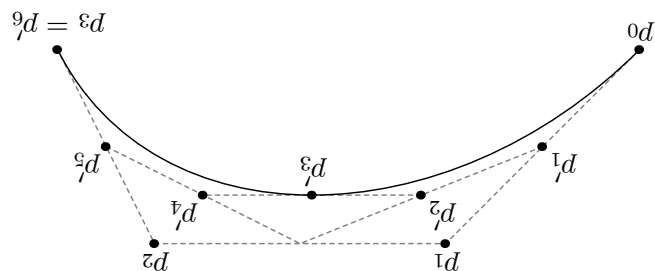
Figure 3.4: A Larger Figure, Flipped Upside Down

Next, we will explore the use of the `out.extra` chunk option, which can be used to shrink or expand an image loaded from a file by specifying `"scale= "`. Here we use the mathematical graph stored in the "subdivision.pdf" file. Here is a reference to this image: Figure 3.3. Note that `echo=FALSE` is specified so that the **R** code is hidden in the document.

More Figure Stuff

Lastly, we will explore how to rotate and enlarge figures using the `out.extra` chunk option. (Currently this only works in the PDF version of the book.) As another example, here is a reference: Figure 3.4.

Footnotes and Endnotes

You might want to footnote something.[1] The footnote will be in a smaller font and placed appropriately. Endnotes work in much the same way.

---

[1]footnote text

Bibliographies

Of course you will need to cite things, and you will probably accumulate an armful of sources. There are a variety of tools available for creating a bibliography database (stored with the .bib extension). In addition to BibTeX suggested below, you may want to consider using the free and easy-to-use tool called Zotero. Some Zotero documentation is at http://libguides.reed.edu/citation/zotero. In addition, a tutorial is available from Middlebury College at http://sites.middlebury.edu/zoteromiddlebury/.

R Markdown uses *pandoc* (http://pandoc.org/) to build its bibliographies. One nice caveat of this is that you won't have to do a second compile to load in references as standard LaTeX requires. To cite references in your thesis (after creating your bibliography database), place the reference name inside square brackets and precede it by the "at" symbol. For example, here's a reference to a book about worrying: (**???**). This `Molina1994` entry appears in a file called `thesis.bib` in the `bib` folder. This bibliography database file was created by a program called BibTeX. You can call this file something else if you like (look at the YAML header in the main .Rmd file) and, by default, is to placed in the `bib` folder.

For more information about BibTeX and bibliographies, see (http://web.reed.edu/cis/help/latex/index.html)[2]. There are three pages on this topic: *bibtex* (which talks about using BibTeX, at http://web.reed.edu/cis/help/latex/bibtex.html), *bibtexstyles* (about how to find and use the bibliography style that best suits your needs, at http://web.reed.edu/cis/help/latex/bibtexstyles.html) and *bibman* (which covers how to make and maintain a bibliography by hand, without BibTeX, at http://web.reed.edu/cis/help/latex/bibman.html). The last page will not be useful un-

---

[2](**???**)

less you have only a few sources.

If you look at the YAML header at the top of the main .Rmd file you can see that we can specify the style of the bibliography by referencing the appropriate csl file. You can download a variety of different style files at `https://www.zotero.org/styles`. Make sure to download the file into the csl folder.

Tips for Bibliographies

- Like with thesis formatting, the sooner you start compiling your bibliography for something as large as thesis, the better.
- The cite key (a citation's label) needs to be unique from the other entries.
- When you have more than one author or editor, you need to separate each author's name by the word "and" e.g. `Author = {Noble, Sam and Youngberg, Jessica},`.
- Bibliographies made using BibTeX (whether manually or using a manager) accept LaTeX markup, so you can italicize and add symbols as necessary.
- To force capitalization in an article title or where all lowercase is generally used, bracket the capital letter in curly braces.

Anything else?

If you'd like to see examples of other things in this template, please contact us (email `rapeek@ucdavis.edu`) with your suggestions. We love to see people using *R Markdown* for their theses, so we'll do our best to help.

Appendix: Supplemental Information for 'Chapter 1: Remote sensing resistance'

Supplemental methods

Normalized difference vegetation index (NDVI; Supplemental Equation 1) correlates with vegetation density, canopy cover, and leaf area index (Rouse et al. 1973). Normalized difference moisture index (NDMI; Supplemental Equation 2) correlates with similar vegetation characteristics as NDVI, but doesn't saturate at high levels of foliar biomass (Gao 1996, Huesca et al. (2016)). Normalized burn ratio (NBR; Supplemental Equation 3) and normalized burn ratio version 2 (NBR2; Supplemental Equation 4) respond strongly to fire effects on vegetation (García and Caselles 1991, Key and Benson 2006, USGS 2017a, 2017b, Hawbaker et al. 2017).

Supplemental Equation 1: $ndvi = (nir - red)/(nir + red)$

Supplemental Equation 2: $ndmi = (nir - swir1)/(nir + swir1)$

Supplemental Equation 3: $nbr = (nir - swir2)/(nir + swir2)$

SUPPLEMENTAL METHODS

Supplemental Equation 4: $nbr2 = (swir1 - swir2)/(swir1 + swir2)$

Where nir is the near infrared band (band 4 on Landsat 4, 5, and 7; band 5 on Landsat 8) and red is the red band (band 3 on Landsat 4, 5, and 7; band 4 on Landsat 8), $swir1$ is the first short wave infrared band (band 5 on Landsat 4, 5, and 7; band 4 on Landsat 8), $swir2$ is the second short wave infrared band (band 7 on Landsat 4, 5, 7, and 8)

We calculated the delta severity indices (dNBR, dNBR2, dNDVI) by subtracting the respective postfire indices from the prefire indices (NBR, NBR2, and NDVI) without multiplying by a rescaling constant (e.g., we did not multiply the result by 1000 as in Miller and Thode (2007); Supplemental Equation 5). Following Reilly et al. (2017), we chose not to correct the delta indices using a phenological offset value (typically calculated as the delta index in homogeneous forest patch outside of the fire perimeter), as our approach implicitly accounts for phenology by incorporating multiple cloud-free images across the same time window both before the fire and one year later.

Supplemental Equation 5: $dI = I_{\text{prefire}} - I_{\text{postfire}}$

We calculated the relative delta severity indices, RdNBR and RdNDVI, by scaling the respective delta indices (dNBR and dNDVI) from Supplemental Equation 6 by a square root transformation of the absolute value of the prefire index.

Supplemental Equation 6: $RdI = \dfrac{dI}{\sqrt{abs(I_{\text{prefire}})}}$

We calculated the relative burn ratio (RBR) following Parks et al. (2014) using Supplemental Equation 7.

Supplemental Equation 7: $RBR = \dfrac{dNBR}{NBR_{\text{prefire}} + 1.001}$

We used the digital elevation model to calculate the potential annual heat load (Supplemental Equation 8 at each pixel, which is an integrated measure of latitude, slope, and a folding transformation of aspect about the northeast-southwest line, such that north-

east becomes 0 radians and southwest becomes π radians (McCune and Keon 2002, with correction in McCune 2007).

(Supplemental Equation 8:

$$aspect_{folded} = abs(\pi - abs(aspect - \frac{5\pi}{4}))$$

$$- 1.467+$$

$$1.582 * cos(latitude)cos(slope)-$$

$$log(pahl) = 1.5 * cos(aspect_{folded})sin(slope)sin(latitude)-$$

$$0.262 * sin(lat)sin(slope)+$$

$$0.607 * sin(aspect_{folded})sin(slope)$$

Where *pahl* is the potential annual heat load, $aspect_{folded}$ is a transformation of aspect in radians, and both *latitude* and *slope* are extracted from a digital elevation model with units of radians.

Supplemental figures and tables

SUPPLEMENTAL FIGURES AND TABLES

Table 3.2: Comparison of models used to validate and calibrate remotely sensed wildfire severity with ground-based composite burn index (CBI) severity sorted in descending order by the R^2 value from a 5-fold cross validation. A total of 56 models were tested representing all possible combinations of 7 different measures of wildfire severity (RBR, dNBR, dNBR2, RdNBR, RdNBR2, dNDVI, and RdNDVI), 4 different time windows in which Landsat imagery was acquired and summarized with a median reducer on a pixel-by-pixel basis (16 days, 32 days, 48 days, and 64 days), and two different interpolation methods (bilinear and bicubic). The three parameters (β_0, β_1, and β_2) from the nonlinear model fit described in Eq. 1 are reported. For each model, the value of the remotely sensed wildfire severity measurement corresponding to the lower bounds of 3 commonly used categories of severity are reported ('low' corresponds to a CBI value of 0.1, 'mod' corresponds to a CBI value of 1.25, and 'high' corresponds to a CBI value of 2.25)

Rank	Severity measure	Time window	Interpolation	k-fold R^2	β_0	β_1	β_2	low	mod	high
1	RBR	48	bicubic	0.82	0.014	0.028	1.001	0.045	0.113	0.282
2	RdNBR	32	bilinear	0.813	-0.483	3.061	0.857	2.852	8.45	20.56
3	RdNDVI	48	bilinear	0.809	-2.144	3.273	0.609	1.335	4.867	10.75

47

Rank	Severity measure	Time window	Interpolation	k-fold R^2	β_0	β_1	β_2	low	mod	high
4	RBR	32	bilinear	0.807	0.014	0.029	0.985	0.046	0.113	0.28
5	RdNDVI	64	bicubic	0.805	-2.524	3.57	0.59	1.263	4.936	10.93
6	RBR	64	bicubic	0.805	0.016	0.027	1.01	0.046	0.113	0.283
7	RdNDVI	32	bicubic	0.803	-2.737	3.308	0.619	0.782	4.436	10.59
8	RBR	64	bilinear	0.802	0.017	0.027	1.003	0.047	0.113	0.279
9	RdNDVI	32	bilinear	0.801	-2.531	3.176	0.624	0.849	4.393	10.39
10	RdNDVI	48	bicubic	0.797	-2.623	3.624	0.587	1.22	4.922	10.94
11	RdNDVI	64	bilinear	0.796	-2.14	3.287	0.607	1.353	4.876	10.73
12	RdNBR	64	bilinear	0.792	-0.42	3.031	0.862	2.884	8.483	20.66
13	RBR	48	bilinear	0.791	0.017	0.027	1.006	0.047	0.112	0.277
14	RBR	32	bicubic	0.79	0.013	0.029	0.994	0.045	0.114	0.284
15	RdNBR	48	bicubic	0.785	-0.858	3.219	0.852	2.647	8.476	21.02
16	RBR	16	bilinear	0.781	0.021	0.026	1.016	0.05	0.114	0.278
17	RdNBR	32	bicubic	0.776	-0.954	3.34	0.841	2.679	8.602	21.2
18	dNDVI	32	bicubic	0.776	-0.058	0.073	0.65	0.02	0.106	0.257
19	dNBR	48	bicubic	0.775	0.03	0.035	1.069	0.068	0.161	0.413
20	RdNBR	16	bilinear	0.774	0.279	2.518	0.909	3.037	8.119	19.73
21	dNDVI	32	bilinear	0.772	-0.053	0.07	0.656	0.022	0.105	0.252
22	dNDVI	48	bicubic	0.772	-0.055	0.081	0.613	0.031	0.119	0.267
23	dNBR	32	bilinear	0.77	0.029	0.036	1.048	0.069	0.163	0.41
24	RdNBR2	64	bicubic	0.766	2.102	0.416	1.24	2.572	4.059	8.861
25	dNBR	32	bicubic	0.764	0.028	0.036	1.057	0.068	0.163	0.417
26	dNDVI	48	bilinear	0.762	-0.044	0.073	0.637	0.034	0.118	0.262

Rank	Severity measure	Time window	Interpolation	k-fold R^2	β_0	β_1	β_2	low	mod	high
27	RBR	16	bicubic	0.761	0.021	0.026	1.028	0.049	0.114	0.281
28	dNBR	16	bilinear	0.76	0.033	0.036	1.048	0.073	0.167	0.417
29	RdNBR2	32	bilinear	0.759	1.435	0.625	1.1	2.132	3.906	8.861
30	RdNBR	16	bicubic	0.758	0.37	2.446	0.926	3.053	8.149	20
31	RdNBR2	32	bicubic	0.754	1.426	0.601	1.125	2.098	3.876	8.975
32	dNBR	64	bicubic	0.753	0.033	0.033	1.086	0.07	0.161	0.413
33	dNBR	64	bilinear	0.751	0.035	0.033	1.08	0.071	0.161	0.406
34	RdNBR2	48	bicubic	0.751	1.835	0.46	1.209	2.354	3.919	8.818
35	dNBR	48	bilinear	0.748	0.035	0.033	1.076	0.071	0.161	0.405
36	RdNDVI	16	bilinear	0.747	-0.983	2.503	0.678	1.695	4.856	10.52
37	dNDVI	64	bicubic	0.746	-0.055	0.082	0.609	0.032	0.12	0.266
38	dNDVI	64	bilinear	0.741	-0.046	0.075	0.627	0.034	0.118	0.261
39	RdNBR2	48	bilinear	0.737	1.802	0.497	1.174	2.361	3.956	8.766
40	RdNBR	64	bicubic	0.737	-1.448	3.651	0.819	2.515	8.717	21.61
41	RdNBR2	64	bilinear	0.735	2.027	0.451	1.204	2.536	4.06	8.801
42	dNBR	16	bicubic	0.729	0.032	0.036	1.058	0.072	0.168	0.423
43	dNBR2	32	bilinear	0.727	0.026	0.009	1.149	0.035	0.062	0.14
44	dNDVI	16	bicubic	0.726	-0.03	0.065	0.674	0.04	0.121	0.267
45	RdNDVI	16	bicubic	0.725	-1.248	2.681	0.665	1.618	4.908	10.72
46	dNBR2	32	bicubic	0.715	0.025	0.008	1.177	0.035	0.061	0.142
47	dNBR2	64	bilinear	0.714	0.036	0.006	1.283	0.043	0.064	0.137
48	dNDVI	16	bilinear	0.707	-0.023	0.06	0.689	0.042	0.12	0.261
49	dNBR2	48	bilinear	0.686	0.033	0.006	1.248	0.04	0.063	0.137

Rank	Severity measure	Time window	Interpolation	k-fold R^2	β_0	β_1	β_2	low	mod	high
50	RdNBR2	16	bilinear	0.682	1.928	0.465	1.189	2.452	3.983	8.676
51	dNBR2	16	bilinear	0.662	0.03	0.009	1.138	0.04	0.066	0.143
52	RdNBR2	16	bicubic	0.654	1.871	0.467	1.198	2.398	3.96	8.792
53	dNBR2	16	bicubic	0.635	0.029	0.009	1.156	0.039	0.066	0.145
54	RdNBR	48	bilinear	0.63	-3.445	5.132	0.724	2.072	9.235	22.7
55	dNBR2	48	bicubic	0	0.033	0.006	1.284	0.04	0.062	0.138
56	dNBR2	64	bicubic	0	0.037	0.005	1.313	0.043	0.064	0.139

Table 3.3: Model parameter estimates for different neighborhood sizes. Values represent the mean parameter estimates with 95% credible intervals in parentheses.

Coefficient	90m x 90m neighborhood	150m x 150m neighborhood	210m x 210m neighborhood	270m x 270m neighborhood
β_0	-2.415 (-2.588, -2.255)	-2.432 (-2.605, -2.271)	-2.447 (-2.619, -2.279)	-2.45 (-2.618, -2.288)
$\beta_{\text{nbhd\_stdev\_NDVI}}$	-0.208 (-0.247, -0.17)	-0.212 (-0.255, -0.17)	-0.203 (-0.248, -0.158)	-0.195 (-0.242, -0.148)

Coefficient	90m x 90m neighborhood	150m x 150m neighborhood	210m x 210m neighborhood	270m x 270m neighborhood
$\beta_{\text{prefire\_NDVI}}$	1.044 (0.911, 1.174)	1.13 (1.028, 1.229)	1.141 (1.057, 1.222)	1.132 (1.056, 1.209)
β_{fm100}	-0.569 (-0.71, -0.423)	-0.564 (-0.709, -0.419)	-0.561 (-0.697, -0.428)	-0.565 (-0.712, -0.422)
β_{pahl}	0.239 (0.208, 0.271)	0.238 (0.205, 0.269)	0.239 (0.207, 0.269)	0.24 (0.209, 0.272)
$\beta_{\text{topographic\_roughness}}$	-0.01 (-0.042, 0.022)	-0.006 (-0.039, 0.027)	-0.002 (-0.037, 0.032)	-0.002 (-0.036, 0.033)
$\beta_{\text{nbhd\_mean\_NDVI}}$	-0.14 (-0.278, 0.002)	-0.265 (-0.381, -0.148)	-0.293 (-0.392, -0.193)	-0.293 (-0.389, -0.198)
$\beta_{\text{nbhd\_stdev\_NDVI*prefire\_NDVI}}$	0.125 (0.029, 0.218)	0.06 (-0.013, 0.135)	0.022 (-0.045, 0.09)	0.009 (-0.054, 0.072)
$\beta_{\text{nbhd\_stdev\_NDVI*nbhd\_mean\_NDVI}}$	-0.129 (-0.223, -0.034)	-0.078 (-0.151, -0.006)	-0.03 (-0.095, 0.035)	-0.006 (-0.068, 0.054)

Coefficient	90m x 90m neighborhood	150m x 150m neighborhood	210m x 210m neighborhood	270m x 270m neighborhood
$\beta_{\text{nbhd\_stdev\_NDVI*fm100}}$	-0.037	-0.035	-0.03	-0.023
	(-0.081,	(-0.078,	(-0.076,	(-0.07,
	0.006)	0.01)	0.014)	0.023)
$\beta_{\text{nbhd\_mean\_NDVI*prefire\_NDVI}}$	-0.573	-0.564	-0.549	-0.537
	(-0.62,	(-0.612,	(-0.596,	(-0.587,
	-0.526)	-0.516)	-0.502)	-0.49)

Figure 3.5: Schematic for how Landsat imagery was assembled in order to make comparisons between pre- and post-fire conditions. This schematic depicts a 64-day window of image collation prior to the fire which comprise the pre-fire image collection. A similar, 64-day window collection of imagery is assembled one year after the pre-fire image collection.
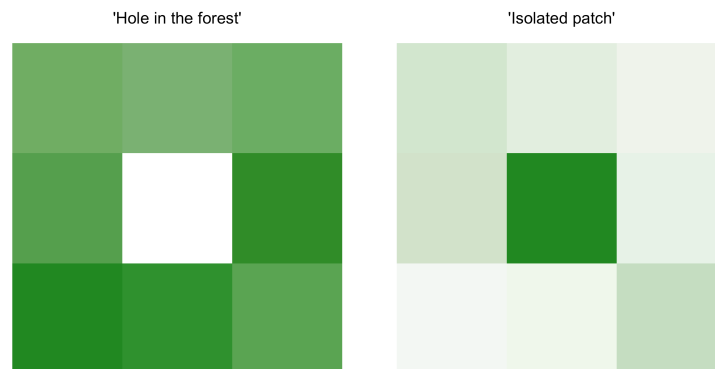
Figure 3.6: Conceptual diagram of 'decoupling' that sometimes occurs between the central pixel NDVI and the neighborhood mean NDVI. In each of these scenarios, our model results suggest that the probability that the central pixel burns at high severity is higher than expected given the additive effect of the covariates. The left panel depicts the "hole in the forest" decoupling, which occurs more frequently, and the right panel depicts the "isolated patch" decoupling.'

References

Abatzoglou, J. T. 2013. Development of gridded surface meteorological data for ecological applications and modelling. International Journal of Climatology 33:121–131.

Ackerly, D. D., S. R. Loarie, W. K. Cornwell, S. B. Weiss, H. Hamilton, R. Branciforte, and N. J. B. Kraft. 2010. The geography of climate change: Implications for conservation biogeography: Geography of climate change. Diversity and Distributions 16:476–487.

Agashe, D. 2009. The Stabilizing Effect of Intraspecific Genetic Variation on Population Dynamics in Novel and Ancestral Habitats. The American Naturalist 174:255–267.

Agee, J. K., and C. N. Skinner. 2005. Basic principles of forest fuel reduction treatments. Forest Ecology and Management 211:83–96.

Agee, J., and C. ForestResourcesU. 1996. The influence of forest structure on fire behavior. 17th Forest Vegetation Management Conference:17.

Asner, G. P., P. G. Brodrick, C. B. Anderson, N. Vaughn, D. E. Knapp, and R. E. Martin. 2016. Progressive forest canopy water loss during the 20122015 California drought. Proceedings of the National Academy of Sciences 113:E249–E255.

Baskett, M. L., S. D. Gaines, and R. M. Nisbet. 2009. Symbiont diversity may help coral

References

reefs survive moderate climate change. Ecological Applications 19:3–17.

Bastarrika, A., E. Chuvieco, and M. P. Martín. 2011. Mapping burned areas from Landsat TM/ETM+ data with a two-phase algorithm: Balancing omission and commission errors. Remote Sensing of Environment 115:1003–1012.

Beck, J., L. Ballesteros-Mejia, C. M. Buchmann, J. Dengler, S. A. Fritz, B. Gruber, C. Hof, F. Jansen, S. Knapp, H. Kreft, A.-K. Schneider, M. Winter, and C. F. Dormann. 2012. What's on the horizon for macroecology? Ecography 35:673–683.

Boschetti, L., D. P. Roy, C. O. Justice, and M. L. Humber. 2015. MODISLandsat fusion for large area 30m burned area mapping. Remote Sensing of Environment 161:27–42.

Bürkner, P.-C. 2017. **Brms** : An *R* Package for Bayesian Multilevel Models Using *Stan*. Journal of Statistical Software 80.

Cadotte, M., C. H. Albert, and S. C. Walker. 2013. The ecology of differences: Assessing community assembly with trait and evolutionary distances. Ecology Letters 16:1234–1244.

Calkin, D. E., K. M. Gebert, J. G. Jones, and R. P. Neilson. 2005. Forest Service Large Fire Area Burned and Suppression Expenditure Trends, 19702002. Journal of Forestry 103:179–183.

Cansler, C. A., and D. McKenzie. 2012. How Robust Are Burn Severity Indices When Applied in a New Region? Evaluation of Alternate Field-Based and Remote-Sensing Methods. Remote Sensing 4:456–483.

Chesson, P. 2000. Mechanisms of Maintenance of Species Diversity. Annual Review of Ecology and Systematics 31:343–366.

Clark, J. S., L. Iverson, C. W. Woodall, C. D. Allen, D. M. Bell, D. C. Bragg, A.

W. D'Amato, F. W. Davis, M. H. Hersh, I. Ibanez, S. T. Jackson, S. Matthews, N. Pederson, M. Peters, M. W. Schwartz, K. M. Waring, and N. E. Zimmermann. 2016. The impacts of increasing drought on forest dynamics, structure, and biodiversity in the United States. Global Change Biology 22:2329–2352.

Collins, B. M., J. M. Lydersen, D. L. Fry, K. Wilkin, T. Moody, and S. L. Stephens. 2016. Variability in vegetation and surface fuels across mixed-conifer-dominated landscapes with over 40 years of natural fire. Forest Ecology and Management 381:74–83.

Coppoletta, M., K. E. Merriam, and B. M. Collins. 2016. Post-fire vegetation and fuel development influences fire severity patterns in reburns. Ecological Applications 26:686–699.

Crowther, T. W., H. B. Glick, K. R. Covey, C. Bettigole, D. S. Maynard, S. M. Thomas, J. R. Smith, G. Hintler, M. C. Duguid, G. Amatulli, M.-N. Tuanmu, W. Jetz, C. Salas, C. Stam, D. Piotto, R. Tavani, S. Green, G. Bruce, S. J. Williams, S. K. Wiser, M. O. Huber, G. M. Hengeveld, G.-J. Nabuurs, E. Tikhonova, P. Borchardt, C.-F. Li, L. W. Powrie, M. Fischer, A. Hemp, J. Homeier, P. Cho, A. C. Vibrans, P. M. Umunay, S. L. Piao, C. W. Rowe, M. S. Ashton, P. R. Crane, and M. A. Bradford. 2015. Mapping tree density at a global scale. Nature 525:201–205.

De Santis, A., G. P. Asner, P. J. Vaughan, and D. E. Knapp. 2010. Mapping burn severity and burning efficiency in California using simulation models and Landsat imagery. Remote Sensing of Environment 114:1535–1545.

Dillon, G. K., Z. A. Holden, P. Morgan, M. A. Crimmins, E. K. Heyerdahl, and C. H. Luce. 2011. Both topography and climate affected forest and woodland burn severity in two regions of the western US, 1984 to 2006. Ecosphere 2:art130.

Edwards, A. C., J. Russell-Smith, and S. W. Maier. 2018. A comparison and validation

References

of satellite-derived fire severity mapping techniques in fire prone north Australian savannas: Extreme fires and tree stem mortality. Remote Sensing of Environment 206:287–299.

Eidenshink, J., B. Schwind, K. Brewer, Z.-L. Zhu, B. Quayle, and S. Howard. 2007. A Project for Monitoring Trends in Burn Severity. Fire Ecology 3:3–21.

Farr, T. G., P. A. Rosen, E. Caro, R. Crippen, R. Duren, S. Hensley, M. Kobrick, M. Paller, E. Rodriguez, L. Roth, D. Seal, S. Shaffer, J. Shimada, J. Umland, M. Werner, M. Oskin, D. Burbank, and D. Alsdorf. 2007. The Shuttle Radar Topography Mission. Reviews of Geophysics 45.

Fernández-García, V., M. Santamarta, A. Fernández-Manso, C. Quintano, E. Marcos, and L. Calvo. 2018. Burn severity metrics in fire-prone pine ecosystems along a climatic gradient using Landsat imagery. Remote Sensing of Environment 206:205–217.

Foga, S., P. L. Scaramuzza, S. Guo, Z. Zhu, R. D. Dilley, T. Beckmann, G. L. Schmidt, J. L. Dwyer, M. Joseph Hughes, and B. Laue. 2017. Cloud detection algorithm comparison and validation for operational Landsat data products. Remote Sensing of Environment 194:379–390.

Franklin, J., T. Logan, C. Woodcock, and A. Strahler. 1986. Coniferous Forest Classification and Inventory Using Landsat and Digital Terrain Data. IEEE Transactions on Geoscience and Remote Sensing GE-24:139–149.

Gao, B.-c. 1996. NDWIA normalized difference water index for remote sensing of vegetation liquid water from space. Remote Sensing of Environment 58:257–266.

García, M. L., and V. Caselles. 1991. Mapping burns and natural reforestation using

thematic Mapper data. Geocarto International 6:31–37.

Gazol, A., and J. J. Camarero. 2016. Functional diversity enhances silver fir growth resilience to an extreme drought. Journal of Ecology 104:1063–1075.

Gelman, A., B. Goodrich, J. Gabry, and A. Vehtari. 2018. R-squared for Bayesian regression models. The American Statistician:1–6.

Goodwin, N. R., and L. J. Collett. 2014. Development of an automated method for mapping fire history captured in Landsat TM and ETM+ time series across Queensland, Australia. Remote Sensing of Environment 148:206–221.

Gorelick, N., M. Hancher, M. Dixon, S. Ilyushchenko, D. Thau, and R. Moore. 2017. Google Earth Engine: Planetary-scale geospatial analysis for everyone. Remote Sensing of Environment 202:18–27.

Graham, R. T., S. McCaffrey, and T. B. Jain. 2004. Science basis for changing forest structure to modify wildfire behavior and severity. U.S. Department of Agriculture, Forest Service, Rocky Mountain Research Station, Ft. Collins, CO.

Hansen, M. C., P. V. Potapov, R. Moore, M. Hancher, S. A. Turubanova, A. Tyukavina, D. Thau, S. V. Stehman, S. J. Goetz, T. R. Loveland, A. Kommareddy, A. Egorov, L. Chini, C. O. Justice, and J. R. G. Townshend. 2013. High-Resolution Global Maps of 21st-Century Forest Cover Change. Science 342:850–853.

Haralick, R. M., K. Shanmugam, and I. Dinstein. 1973. Textural Features for Image Classification. IEEE Transactions on Systems, Man, and Cybernetics SMC-3:610–621.

Hawbaker, T. J., M. K. Vanderhoof, Y.-J. Beal, J. D. Takacs, G. L. Schmidt, J. T. Falgout, B. Williams, N. M. Fairaux, M. K. Caldwell, J. J. Picotte, S. M. Howard,

References

S. Stitt, and J. L. Dwyer. 2017. Mapping burned areas using dense time-series of Landsat data. Remote Sensing of Environment 198:504–522.

Heffernan, J. B., P. A. Soranno, M. J. Angilletta, L. B. Buckley, D. S. Gruner, T. H. Keitt, J. R. Kellner, J. S. Kominoski, A. V. Rocha, J. Xiao, T. K. Harms, S. J. Goring, L. E. Koenig, W. H. McDowell, H. Powell, A. D. Richardson, C. A. Stow, R. Vargas, and K. C. Weathers. 2014. Macrosystems ecology: Understanding ecological patterns and processes at continental scales. Frontiers in Ecology and the Environment 12:5–14.

Henry, L., and H. Wickham. 2019. Purrr: Functional Programming Tools.

Hoffman, M. D., and A. Gelman. 2014. The No-U-Turn Sampler: Adaptively Setting Path Lengths in Hamiltonian Monte Carlo. Journal of Machine Learning Research 15:31.

Holden, Z. A., P. Morgan, and J. S. Evans. 2009. A predictive model of burn severity based on 20-year satellite-inferred burn severity data in a large southwestern US wilderness area. Forest Ecology and Management 258:2399–2406.

Holling, C. S. 1973. Resilience and Stability of Ecological Systems. Annual Review of Ecology and Systematics:1–23.

Huang, Q., A. Swatantran, R. Dubayah, and S. J. Goetz. 2014. The Influence of Vegetation Height Heterogeneity on Forest and Woodland Bird Species Richness across the United States. PLoS ONE 9:e103236.

Huesca, M., M. García, K. L. Roth, A. Casas, and S. L. Ustin. 2016. Canopy structural attributes derived from AVIRIS imaging spectroscopy data in a mixed

broadleaf/conifer forest. Remote Sensing of Environment 182:208–226.

JepsonFloraProject, editor. 2016. Jepson eFlora.

Keith, D. A., J. P. Rodríguez, K. M. Rodríguez-Clark, E. Nicholson, K. Aapala, A. Alonso, M. Asmussen, S. Bachman, A. Basset, E. G. Barrow, J. S. Benson, M. J. Bishop, R. Bonifacio, T. M. Brooks, M. A. Burgman, P. Comer, F. A. Comín, F. Essl, D. Faber-Langendoen, P. G. Fairweather, R. J. Holdaway, M. Jennings, R. T. Kingsford, R. E. Lester, R. M. Nally, M. A. McCarthy, J. Moat, M. A. Oliveira-Miranda, P. Pisanu, B. Poulin, T. J. Regan, U. Riecken, M. D. Spalding, and S. Zambrano-Martínez. 2013. Scientific Foundations for an IUCN Red List of Ecosystems. PLoS ONE 8:e62111.

Key, C. H., and N. C. Benson. 2006. Landscape Assessment (LA):55.

Kéfi, S., V. Guttal, W. A. Brock, S. R. Carpenter, A. M. Ellison, V. N. Livina, D. A. Seekell, M. Scheffer, E. H. van Nes, and V. Dakos. 2014. Early Warning Signals of Ecological Transitions: Methods for Spatial Patterns. PLoS ONE 9:e92097.

Kolden, C. A., A. M. S. Smith, and J. T. Abatzoglou. 2015. Limitations and utilisation of Monitoring Trends in Burn Severity products for assessing wildfire severity in the USA. International Journal of Wildland Fire 24:1023.

Kotliar, N. B., and J. A. Wiens. 1990. Multiple Scales of Patchiness and Patch Structure: A Hierarchical Framework for the Study of Heterogeneity. Oikos 59:253.

Larson, A. J., and D. Churchill. 2012. Tree spatial patterns in fire-frequent forests of western North America, including mechanisms of pattern formation and implications for designing fuel reduction and restoration treatments. Forest Ecology and Manage-

References

ment 267:74–92.

Lenoir, J., B. J. Graae, P. A. Aarrestad, I. G. Alsos, W. S. Armbruster, G. Austrheim, C. Bergendorff, H. J. B. Birks, K. A. Bråthen, J. Brunet, H. H. Bruun, C. J. Dahlberg, G. Decocq, M. Diekmann, M. Dynesius, R. Ejrnaes, J.-A. Grytnes, K. Hylander, K. Klanderud, M. Luoto, A. Milbau, M. Moora, B. Nygaard, A. Odland, V. T. Ravolainen, S. Reinhardt, S. M. Sandvik, F. H. Schei, J. D. M. Speed, L. U. Tveraabak, V. Vandvik, L. G. Velle, R. Virtanen, M. Zobel, and J.-C. Svenning. 2013. Local temperatures inferred from plant communities suggest strong spatial buffering of climate warming across Northern Europe. Global Change Biology 19:1470–1481.

Lydersen, J. M., B. M. Collins, E. E. Knapp, G. B. Roller, and S. Stephens. 2015. Relating fuel loads to overstorey structure and composition in a fire-excluded Sierra Nevada mixed conifer forest. International Journal of Wildland Fire 24:484.

Lydersen, J. M., M. P. North, and B. M. Collins. 2014. Severity of an uncharacteristically large wildfire, the Rim Fire, in forests with relatively restored frequent fire regimes. Forest Ecology and Management 328:326–334.

Malone, S., P. Fornwalt, M. Battaglia, M. Chambers, J. Iniguez, and C. Sieg. 2018. Mixed-Severity Fire Fosters Heterogeneous Spatial Patterns of Conifer Regeneration in a Dry Conifer Forest. Forests 9:45.

Masek, J., E. Vermote, N. Saleous, R. Wolfe, F. Hall, K. Huemmrich, F. Gao, J. Kutler, and T.-K. Lim. 2006. A Landsat Surface Reflectance Dataset for North America, 19902000. IEEE Geoscience and Remote Sensing Letters 3:68–72.

McCune, B. 2007. Improved estimates of incident radiation and heat load using nonparametric regression against topographic variables. Journal of Vegetation Science

18:751–754.

McCune, B., and D. Keon. 2002. Equations for potential annual direct incident radiation and heat load. Journal of Vegetation Science 13:603–606.

Millar, C. I., and N. L. Stephenson. 2015. Temperate forest health in an era of emerging megadisturbance. Science 349:823–826.

Millar, C. I., N. L. Stephenson, and S. L. Stephens. 2007. CLIMATE CHANGE AND FORESTS OF THE FUTURE: MANAGING IN THE FACE OF UNCERTAINTY. Ecological Applications 17:2145–2151.

Miller, J. D., and H. Safford. 2012. TRENDS IN WILDFIRE SEVERITY: 1984 TO2010 IN THE SIERRA NEVADA, MODOC PLATEAU, AND SOUTHERN CASCADES, CALIFORNIA, USA. Fire Ecology 8:41–57.

Miller, J. D., and H. D. Safford. 2017. Corroborating Evidence of a Pre-Euro-American Low- to Moderate-Severity Fire Regime in Yellow PineMixed Conifer Forests of the Sierra Nevada, California, USA. Fire Ecology 13:58–90.

Miller, J. D., and A. E. Thode. 2007. Quantifying burn severity in a heterogeneous landscape with a relative version of the delta Normalized Burn Ratio (dNBR). Remote Sensing of Environment 109:66–80.

Miller, J. D., E. E. Knapp, C. H. Key, C. N. Skinner, C. J. Isbell, R. M. Creasy, and J. W. Sherlock. 2009. Calibration and validation of the relative differenced Normalized Burn Ratio (RdNBR) to three measures of fire severity in the Sierra Nevada and Klamath Mountains, California, USA. Remote Sensing of Environment 113:645–656.

Miller, J. D., C. N. Skinner, H. D. Safford, E. E. Knapp, and C. M. Ramirez. 2012. Trends and causes of severity, size, and number of fires in northwestern California,

References

USA. Ecological Applications 22:184–203.

Moritz, M. A., M. E. Morais, L. A. Summerell, J. M. Carlson, and J. Doyle. 2005. Wildfires, complexity, and highly optimized tolerance. Proceedings of the National Academy of Sciences 102:17912–17917.

North, M., P. Stine, K. O'Hara, W. Zielinski, and S. Stephens. 2009. An ecosystem management strategy for Sierran mixed-conifer forests. U.S. Department of Agriculture, Forest Service, Pacific Southwest Research Station, Albany, CA.

Parks, S. A., L. M. Holsinger, M. H. Panunto, W. M. Jolly, S. Z. Dobrowski, and G. K. Dillon. 2018. High-severity fire: Evaluating its key drivers and mapping its probability across western US forests. Environmental Research Letters 13:044037.

Parks, S., G. Dillon, and C. Miller. 2014. A New Metric for Quantifying Burn Severity: The Relativized Burn Ratio. Remote Sensing 6:1827–1844.

Peters, D. P. C., R. A. Pielke, B. T. Bestelmeyer, C. D. Allen, S. Munson-McGee, and K. M. Havstad. 2004. Cross-scale interactions, nonlinearities, and forecasting catastrophic events. Proceedings of the National Academy of Sciences 101:15130–15135.

Prichard, S. J., and M. C. Kennedy. 2014. Fuel treatments and landform modify landscape patterns of burn severity in an extreme fire event. Ecological Applications 24:571–590.

Questad, E. J., and B. L. Foster. 2008. Coexistence through spatio-temporal heterogeneity and species sorting in grassland plant communities. Ecology Letters 11:717–726.

R Core Team. 2018. R: A Language and Environment for Statistical Computing. R

Foundation for Statistical Computing, Vienna, Austria.

Reilly, M. J., C. J. Dunn, G. W. Meigs, T. A. Spies, R. E. Kennedy, J. D. Bailey, and K. Briggs. 2017. Contemporary patterns of fire extent and severity in forests of the Pacific Northwest, USA (1985-2010). Ecosphere 8:e01695.

Reusch, T. B. H., A. Ehlers, A. Hammerli, and B. Worm. 2005. Ecosystem recovery after climatic extremes enhanced by genotypic diversity. Proceedings of the National Academy of Sciences 102:2826–2831.

Rouse, W., R. H. Haas, W. Deering, and J. A. Schell. 1973. MONITORING THE VERNAL ADVANCEMENT AND RETROGRADATION (GREEN WAVE EFFECT) OF NATURAL VEGETATION. Type II Report, Goddard Space Flight Center, Greenbelt, MD, USA.

Safford, H. D., and J. T. Stevens. 2017. Natural Range of Variation for Yellow Pine and Mixed-Conifer Forests in the Sierra Nevada, Southern Cascades, and Modoc and Inyo National Forests, California, USA. Page 241.

Safford, H., J. Stevens, K. Merriam, M. Meyer, and A. Latimer. 2012. Fuel treatment effectiveness in California yellow pine and mixed conifer forests. Forest Ecology and Management 274:17–28.

Scholl, A. E., and A. H. Taylor. 2010. Fire regimes, forest change, and self-organization in an old-growth mixed-conifer forest, Yosemite National Park, USA. Ecological Applications 20:362–380.

Sikkink, P. G., G. K. Dillon, R. E. Keane, P. Morgan, E. C. Karau, Z. A. Holden, and R. P. Silverstein. 2013. Composite Burn Index (CBI) data and field photos collected

References

for the FIRESEV project, western United States.

Steel, Z. L., M. J. Koontz, and H. D. Safford. 2018. The changing landscape of wildfire: Burn pattern trends and implications for California's yellow pine and mixed conifer forests. Landscape Ecology 33:1159–1176.

Stein, A., K. Gerstner, and H. Kreft. 2014. Environmental heterogeneity as a universal driver of species richness across taxa, biomes and spatial scales. Ecology Letters 17:866–880.

Stephens, S. L., D. L. Fry, and E. Franco-Vizcaíno. 2008. Wildfire and Spatial Patterns in Forests in Northwestern Mexico: The United States Wishes It Had Similar Fire Problems. Ecology and Society 13.

Stephens, S. L., J. D. McIver, R. E. J. Boerner, C. J. Fettig, J. B. Fontaine, B. R. Hartsough, P. L. Kennedy, and D. W. Schwilk. 2012. The Effects of Forest Fuel-Reduction Treatments in the United States. BioScience 62:549–560.

Stephens, S. L., J. J. Moghaddas, C. Edminster, C. E. Fiedler, S. Haase, M. Harrington, J. E. Keeley, E. E. Knapp, J. D. McIver, K. Metlen, C. N. Skinner, and A. Youngblood. 2009. Fire treatment effects on vegetation structure, fuels, and potential fire severity in western U.S. forests. Ecological Applications 19:305–320.

Stevens, J. T., B. M. Collins, J. D. Miller, M. P. North, and S. L. Stephens. 2017. Changing spatial patterns of stand-replacing fire in California conifer forests. Forest Ecology and Management 406:28–36.

Sugihara, N. G., J. W. V. Wagtendonk, J. Fites-Kaufman, K. E. Shaffer, and A. E. Thode. 2006. Fire in California's ecosystems. University of California Press.

Tilman, D. 1994. Competition and Biodiversity in Spatially Structured Habitats. Ecol-

ogy 75:2–16.

Trumbore, S., P. Brando, and H. Hartmann. 2015. Forest health and global change. Science 349:814–818.

Tuanmu, M.-N., and W. Jetz. 2015. A global, remote sensing-based characterization of terrestrial habitat heterogeneity for biodiversity and ecosystem modelling: Global habitat heterogeneity. Global Ecology and Biogeography 24:1329–1339.

USGS. 2017a. Landsat 8 Surface Reflectance Code (LASRC) Product Guide:40.

USGS. 2017b. Landsat 4-7 Surface Reflectance (LEDAPS) Product Guide:41.

Vehtari, A., A. Gelman, and J. Gabry. 2017. Practical Bayesian model evaluation using leave-one-out cross-validation and WAIC. Statistics and Computing 27:1413–1432.

Veraverbeke, S., and S. J. Hook. 2013. Evaluating spectral indices and spectral mixture analysis for assessing fire severity, combustion completeness and carbon emissions. International Journal of Wildland Fire 22:707.

Vermote, E., C. Justice, M. Claverie, and B. Franch. 2016. Preliminary analysis of the performance of the Landsat 8/OLI land surface reflectance product. Remote Sensing of Environment 185:46–56.

Virah-Sawmy, M., L. Gillson, and K. J. Willis. 2009. How does spatial heterogeneity influence resilience to climatic changes? Ecological dynamics in southeast Madagascar. Ecological Monographs 79:557–574.

Wagner, C. E. V. 1977. Conditions for the start and spread of crown fire. Canadian

Journal of Forest Research 7:23–34.

Wagtendonk, J. W. V. 2006. Fire as a Physical Process. University of California Press.

Walker, B., C. S. Holling, S. R. Carpenter, and A. P. Kinzig. 2004. Resilience, Adaptability and Transformability in Social-ecological Systems. Ecology and Society 9.

Walker, R. B., J. D. Coop, S. A. Parks, and L. Trader. 2018. Fire regimes approaching historic norms reduce wildfire-facilitated conversion from forest to non-forest. Ecosphere 9:e02182.

Wickham, H. 2019. Modelr: Modelling Functions that Work with the Pipe.

Williams, A. P., C. D. Allen, A. K. Macalady, D. Griffin, C. A. Woodhouse, D. M. Meko, T. W. Swetnam, S. A. Rauscher, R. Seager, H. D. Grissino-Mayer, J. S. Dean, E. R. Cook, C. Gangodagamage, M. Cai, and N. G. McDowell. 2013. Temperature as a potent driver of regional forest drought stress and tree mortality. Nature Climate Change 3:292–297.

Wood, E. M., A. M. Pidgeon, V. C. Radeloff, and N. S. Keuler. 2012. Image texture as a remotely sensed measure of vegetation structure. Remote Sensing of Environment 121:516–526.

Young, D. J. N., J. T. Stevens, J. M. Earles, J. Moore, A. Ellis, A. L. Jirka, and A. M. Latimer. 2017. Long-term climate and competition explain forest mortality patterns under extreme drought. Ecology Letters 20:78–86.

Zhu, Z., C. Key, D. Ohlen, and N. Benson. 2006. Evaluate Sensitivities of Burn-Severity Mapping Algorithms for Different Ecosystems and Fire Histories in the United States. Page 35. Final Report to the Joint Fire Science Program.